Hydrothermal equalibria and ore formation

Alekseyev V.A. Colloidal transfer of metals by hydrothermal solutions.

Vernadsky Institute of Geochemistry and Analytical Chemistry RAS, Moscow (alekseyev-v@geokhi.ru)

Abstract. Numerous studies have shown that metals are transported by surface and underground waters not so much in truly dissolved as in colloidal form. Metal colloids (MC) are also formed in hydrothermal solutions during their heterogenization or mixing, which causes supersaturation and nucleation. The formation of MC has been confirmed in hydrothermal experiments, in ores and near ores, in gas-liquid inclusions of minerals, in modern hydrothermal vents. On the example of the silica-water system, the conditions for the formation of MC, their stability and long-distance transport are shown. However, the transfer of metals by supersaturated hydrothermal solutions in which colloids have not yet had time to form may be more effective. Further research in this direction will complement the traditional ideas about the transfer of ore elements by transferring them in the form of supersaturated and colloidal solutions, as well as new mechanisms for the concentration of colloids into ore bodies.

Analyses of natural waters are preceded by their filtration through filters with a pore size of 0.45 microns. Previously, it was assumed that this procedure allows you to attribute the results of analysis of solutions to truly dissolved forms. Later it turned out that this assumption is incorrect for micro-components, because they are often part of colloidal particles that pass through the pores of the filter. Progress in the study of the shape, size, composition and structure of colloidal particles, as well as their transport properties, occurred as a result of the application of new research methods (Ivaneev et al., 2021). It turned out that colloidal transfer of metals in surface and underground waters is a widespread phenomenon (Gottselig et al., 2020; Sasamoto, Onda, 2019). The main colloidal carriers of metals are organics, Fe(III) hydroxides, clays and silica (Dinu, Shkinev, 2020; Baalousha et al., 2011). Some researchers extended colloidal transfer to the hydrothermal process (Chukhrov, 1966), based mainly on the presence of collomorphic forms of minerals. If metals are considered hazardous elements in surface waters, then in hydrothermal solutions they are considered as useful elements capable of concentrating into ore bodies. This paper analyzes new data on this topic.

Collomorphic forms of minerals are considered proof of the participation of colloids (gels) in the formation of minerals based on the similarity of convex forms of minerals and liquids under the action of surface tension (Chukhrov, 1966). However, there is still no convincing evidence of the formation of collomorphic minerals by gel compaction, although the formation of the gel itself (for example, silica) has been observed along the shores of solfatary lakes as a result of evaporation of hot silica-containing solutions (Naboko, 1959). The fact is that minerals crystallize from amorphous substances (including gels) by the dissolution-crystallization mechanism, i.e. through the stage of complete dissolution (disappearance) of the initial substance (Williams, Crerar, 1985).

However, there are numerous evidences of hydrothermal formation of mineral particles, which due to their small size (1-1000 nm) belong to colloids. For example, Au-rich ores often form aggregates consisting entirely of Au nanoparticles (McLeish et al., 2021). Nanoparticles of Au and other minerals are often present in pyrite (Franchini et al., 2015). Au nanoparticles in high concentration (750 mg/kg) were found in fluid inclusions in quartz (Prokofiev et al., 2020). Nanoparticles with high concentrations of Pb, Zn, Cu were found in soil, groundwater and geogas above concealed ore bodies (Liu et al., 2019a). Intensive formation of colloidal particles, mainly metal sulfides, occurs when hot hydrothermal solutions are mixed with cold seawater on the ocean floor in spreading and subduction zones (Gartman et al., 2019). At a geothermal deposit in Iceland, the concentration of colloidal gold in a solution taken from deep wells increased from 3 to 14 mg/kg over 7 years (Hannington et al., 2016). When hydrothermal solutions reach the surface, they cool and become supersaturated, which leads, in particular, to the formation of colloidal silica (Dixit et al., 2016).

It follows from the facts listed above that colloidal particles do exist in hydrothermal solutions. Their appearance is associated with nucleation in supersaturated solutions formed as a result of rapid change in T, P, pH during heterogenization of fluids or mixing of deep and surface waters. However, are they able to move in a fractured-porous medium over long distances and make a significant contribution to the transfer of metals?

The halos of Fe-containing colloids freely propagate in seawater up to 100 km from the place of their formation from "black smokers" (Hoffman et al., 2018). However, in hydrothermal systems located in the Earth's crust, the stability (mobility) of colloids depends on the ratio of their size to the size of pores or fractures through which the hydrothermal solution is filtered. Smaller colloids may be more mobile from this point of view. The stability of colloids also depends on the ratio of attraction and repulsion forces between the particles, which is solved in the DLVO theory. Calculations using this theory have shown that increasing pressure and temperature

respectively stabilize and destabilize colloids (Barton, 2019). This conclusion can be significantly corrected by taking into account forces that were not considered in DLVO theory: hydration, hydrophobic, steric, and bridging forces (Baalousha et al., 2011). Colloidal Au solutions obtained in the reaction of $HAuCl_4$ with H_2O_2 and K_2CO_3 were stable up to 350°C (Frondel, 1938). In a hydrogen sulfide solution, colloidal Au particles with sizes of 10-20 nm and concentrations up to 95 mg/kg were stable up to 300°C (Liu et al., 2019b). Although the duration of these experiments was limited (2.5 and 22 h), a stabilizing effect of SiO_2 colloids on Au colloids was observed in both cases.

Let us consider in more detail the kinetic and transport features of colloids on the example of the most studied silica (SiO_2) colloids, which are formed as a result of polymerization of monomeric (truly dissolved) SiO_2 in supersaturated solutions. Polymerization is preceded by an induction period of maturation of critical nuclear. Its duration increases with a decrease in the degree of supersaturation and ionic strength of the solution, with an increase in temperature and with a pH deviation from the neutral value (Dixit et al., 2016; Icopini et al., 2005). In experiments, the induction period usually does not exceed 2 hours (Dixit et al., 2016), but in natural waters of geothermal sources it can be much larger (White et al., 1956). The stability of supersaturated solutions in the induction period is used to predict the temperature of a deep geothermal reservoir by the composition of the solution that pours from it to the surface and by the temperature dependence of quartz solubility (Arnórsson, 1975). Kinetic modeling has shown that this case is possible only with a small ratio of the quartz surface area to the water mass and/or with a high filtration rate of the solution (Fig. 1).
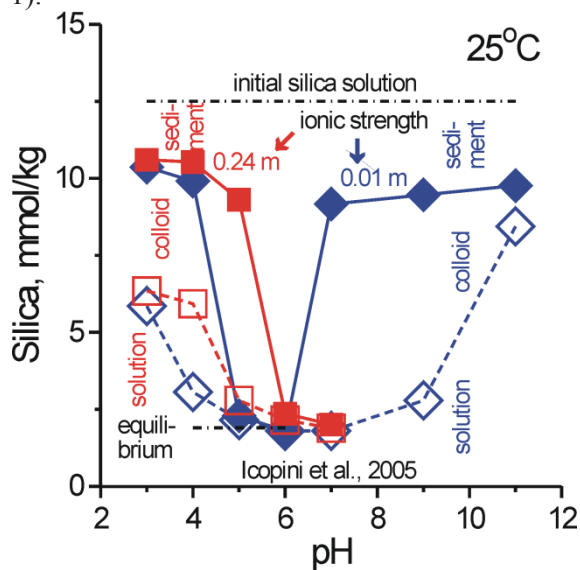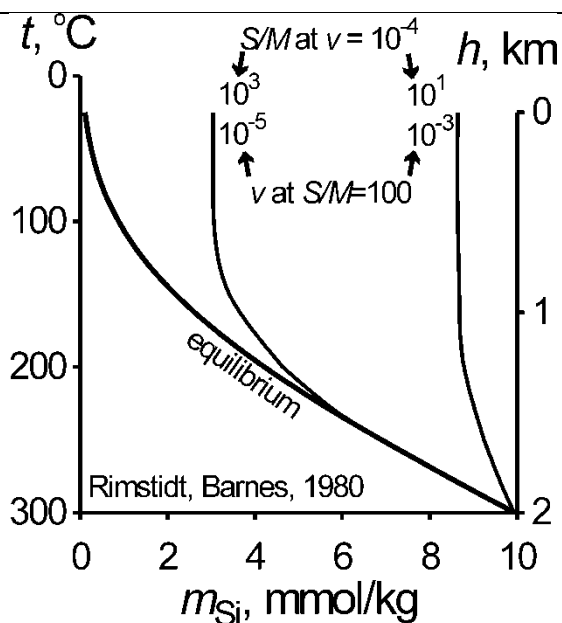

Fig. 1. Change in SiO_2 concentration in solution during ascent to the surface. S/M is the ratio of the surface area of quartz to the mass of water (m²/kg), v is the rate of rise of the solution (m/s).

In this simulation, however, the possibility of SiO_2 polymerization was not taken into account. Polymerization proceeds rapidly in a near neutral solution up to the formation of an amorphous SiO_2 precipitate, but it slows down sharply when the pH deviates into an acidic or alkaline region (Fig. 2). At pH 3, for example, the concentration of colloids was the same in solutions with low and high ionic strength (Fig. 2) and did not change until 4 and 117 days, respectively. A case is described when the SiO_2 sol (30%) with particles of 15 nm in size remained stable at 20-30°C and pH 9-10 for 20 years (Iler, 1979).

Fig. 2. Concentrations of stable forms of SiO_2 in artificial solution depending on pH and ionic strength.
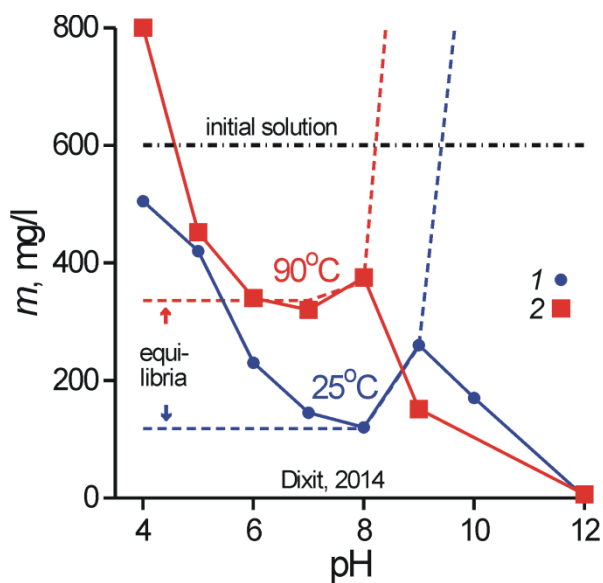

Fig. 3. The concentration of monomeric silica (m) in a natural solution after 9 hours of exposure at 25 (*1*), 90°C (*2*) and different pH.

Institute of Experimental Mineralogy

Polymerization of SiO_2 in a natural hydrothermal solution at 90°C and pH 6-8 leads to a decrease in the concentration of truly dissolved silica (m) to the equilibrium concentration (m_{eq}) after 9 hours (Fig. 3). In contrast to the pure water-silica system (Fig. 2), here at pH > 8-9, the value of m becomes significantly less than m_{eq}, which is explained by the deposition of Ca silicates, and at pH 4 and 90°C, the value of m becomes higher than the initial concentration (Fig. 3). The latter circumstance is explained by the depolymerization of SiO_2 and means that colloidal silica was in solution even before its extraction from the well and rose with solution from the deep geothermal reservoir.

The next step, bringing the experimental conditions closer to natural ones, was passing a hydrothermal solution supersaturated relative to amorphous silica through a long reactor filled with sand (Carroll et al., 1998). However, under these conditions, only a small supersaturation of the solution was created (<2), so amorphous silica was deposited, but colloids were not formed.

Natural hydrothermal solutions pouring onto the surface contain silica mainly in monomeric form. However, the content of this form is somewhat less than the total SiO_2 content, especially at higher concentrations (Fig. 4). The difference in these concentrations indicates the presence of SiO_2 colloids with a content of up to 30 mg/l. It is obvious that these colloids were formed on the path of the rise of hydrothermal solutions and moved with them. The possibility of moving colloids by hydrothermal solutions is also confirmed by the presence of colloids in groundwater, which are filtered through a similar fractured-porous space of rocks. For example, water oozing from mudstone walls of mines in Japan constantly contains colloidal particles up to 500 nm in size with a concentration of up to 4 mg/l (Sasamoto, Onda, 2019). The same low level, but for the total concentrations of Cu and Zn, was found in deep hydrothermal solutions of New Zealand (Simmons et al., 2016). Thermodynamic calculations, however, have shown that these low concentrations correspond to high supersaturation relative to chalcopyrite and sphalerite (hundreds of times). On this basis, the authors assumed the existence of colloidal particles of these minerals, which provided the main contribution to the analysis of solutions (ICP-MS method).

Thus, hydrothermal solutions are capable of transferring metals in much higher concentrations than follows from the traditional approach based on equilibrium thermodynamics. This ability is provided by colloids and supersaturated solutions, and the latter are more mobile.

Colloidal Au and SiO_2 particles play an important role in the formation of epithermal Au deposits not only as an intermediate stage of deposition, but also in the movement of Au and in the concentration of rich ore bodies (Saunders, Burke, 2017). In particular, small pores and cracks in this process can act as filters that allow true solutions to pass through, but delay and accumulate colloidal Au particles. The continuation of experimental, theoretical and field studies in this area will allow us to more accurately assess the role of colloids and supersaturated solutions in the transfer of metals and in the formation of ore deposits.
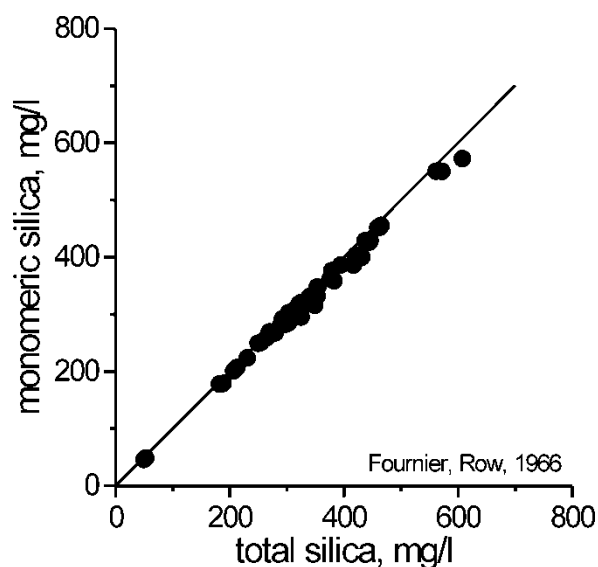

Fig. 4. The concentration of total and monomeric silica in the hot springs of Yellowstone National Park (USA).

References

Arnórsson S. Application of the silica geothermometer in low temperature hydrothermal areas in Iceland // Am. J. Sci. 1975. Vol. 275. No 7. P. 763-784.

Baalousha M., Lead J.R., Ju-Nam Y. Natural colloids and manufactured nanoparticles in aquatic and terrestrial systems // Treatise on Water Sci. 2011. Vol. 3. P. 89-129.

Barton I. The effects of temperature and pressure on the stability of mineral colloids // Amer. J. Sci. 2019. Vol. 319. No 9. P. 737-753.

Carroll S., Mroczek E., Alai M., Ebert M. Amorphous silica precipitation (60 to 120°C): Comparison of laboratory and field rates // Geochim. Cosmochim. Acta. 1998. Vol. 62. No 8. P. 1379-1396.

Chukhrov F.V. Present views on colloids in ore formation // Int. Geol. Rev. 1966. Vol. 8. No 3. P. 336-345.

Dinu M.I., Shkinev V.M. Complexation of metal ions with organic substances of humus nature: Methods of study and structural features of ligands, and distribution of elements between species // Geochem. Int. 2020. Vol. 58. No 2. P. 200-211.

Dixit C. Etude physico-chimique des fluides produits par la centrale géothermique de Bouillante (Guadeloupe) et des dépôts susceptibles de se former au cours de leur refroidissement. Ph.D. Thesis. Antilles-Guyane University, France. 2014. 254 p.

Dixit C., Bernard M.-L., Sanjuan B., André L., Gaspard S. Experimental study on the kinetics of silica polymerization during cooling of the Bouillante geothermal fluid (Guadeloupe, French West Indies) // Chem. Geol. 2016. Vol. 442. P. 97-112.

Fournier R.O., Rowe J.J. Estimation of underground temperatures from the silica content of water from hot springs and wet-steam wells // Am. J. Sci. 1966. Vol. 264. No 9. P. 685-697.

Franchini M., McFarlane C., Maydagán L., Reich M., Lentz D.R., Meinert L., Bouhier V. Trace metals in pyrite and marcasite from the Agua Rica porphyry-high sulfidation epithermal deposit, Catamarca, Argentina: Textural features and metal zoning at the porphyry to epithermal transition // Ore Geol. Rev. 2015. Vol. 66. P. 366-387.

Frondel C. Stability of colloidal gold under hydrothermal conditions // Econ. Geol. 1938. Vol. 33. No 1. P. 1-20.

Gartman A., Findlay A.J., Hannington M., Garbe-Schönberg D., Jamieson J.W., Kwasnitschka T. The role of nanoparticles in mediating element deposition and transport at hydrothermal vents // Geochim. Cosmochim. Acta. 2019. Vol. 261. P. 113-131.

Gottselig N., Sohrt J., Uhlig D., Nischwitz V., Weiler M., Amelung W. Groundwater controls on colloidal transport in forest stream waters // Sci. Total Environ. 2020. Vol. 717. art. 134638.

Hannington M., Hardardóttir V., Garbe-Schönberg D., Brown K.L. Gold enrichment in active geothermal systems by accumulating colloidal suspensions // Nat. Geosci. 2016. Vol. 9. No 4. P. 299-302.

Hoffman C.L., Nicholas S.L., Ohnemus D.C., Fitzsimmons J.N., Sherrell R.M., German C.R., Heller M.I., Lee J.-M., Lam P.J., Toner B.M. Near-field iron and carbon chemistry of non-buoyant hydrothermal plume particles, Southern East Pacific Rise 15°S // Mar. Chem. 2018. Vol. 201. P. 183-197.

Icopini G.A., Brantley S.L., Heaney P.J. Kinetics of silica oligomerization and nanocolloid formation as a function of pH and ionic strength at 25°C // Geochim. Cosmochim. Acta. 2005. Vol. 69. No 2. P. 293-303.

Iler R.K. The Chemistry of Silica: Solubility, Polymerization, Colloid and Surface Properties and Biochemistry of Silica. New York: Wiley, 1979.

Ivaneev A.I., Ermolin M.S., Fedotov P.S. Separation, characterization, and analysis of environmental nano- and microparticles: State-of-the-art methods and approaches // J. Anal. Chem. 2021. Vol. 76. No 4. P. 413-429.

Liu X., Cao J., Li Y., Hu G., Wang G. A study of metal-bearing nanoparticles from the Kangjiawan Pb-Zn deposit and their prospecting significance // Ore Geol. Rev. 2019a. Vol. 105. P. 375-386.

Liu W., Chen M., Yang Y., Mei Y., Etschmann B., Brugger J., Johannessen B. Colloidal gold in sulphur and citrate-bearing hydrothermal fluids: An experimental study // Ore Geol. Rev. 2019b. Vol 114. art. 103142.

McLeish D.F., Williams-Jones A.E., Vasyukova O.V., Clark J.R., Board W.S. Colloidal transport and flocculation are the cause of the hyperenrichment of gold in nature // Proc. Natl. Acad. Sci. U. S. A. 2021. Vol. 118. No 20. art. e2100689118.

Naboko S.I. Volcanic exhalations and products of their reactions. Moscow: USSR Academy of Sciences. 1959. 301 p. (in Russian).

Prokofiev V.Y., Banks D.A., Lobanov K.V., Selektor S.L., Milichko V.A., Akinfiev N.N., Borovikov A.A., Lüders V., Chicherov M.V. Exceptional concentrations of gold nanoparticles in 1.7 Ga fluid inclusions from the Kola superdeep borehole, Northwest Russia // Sci. Rep. 2020. Vol. 10. No 1. art. 1108.

Rimstidt J.D., Barnes H.L. The kinetics of silica–water reactions // Geochim. Cosmochim. Acta. 1980. Vol. 44. No 11. P. 1683-1699.

Sasamoto H., Onda S. Preliminary results for natural groundwater colloids in sedimentary rocks of the horonobe underground research laboratory, Hokkaido, Japan // Geol. Soc. Spec. Publ. 2019. Vol. 482. No 1. P. 191-203.

Saunders J.A., Burke M. Formation and aggregation of gold (Electrum) nanoparticles in epithermal ores // Minerals. 2017. Vol. 7. No 9. art. 163.

Simmons S.F., Brown K.L., Tutolo B.M. Hydrothermal transport of Ag, Au, Cu, Pb, Te, Zn, and other metals and metalloids in New Zealand geothermal systems: Spatial Patterns, Fluid-mineral equilibria, and implications for epithermal mineralization // Econ. Geol. 2016. Vol. 111. No 3. P. 589-618.

White D.E., Brannock W.W., Murata K.J. Silica in hot-spring waters // Geochim. Cosmochim. Acta. 1956. Vol. 10. No 1-2. P. 27-59.

Williams L.A., Crerar D.A. Silica diagenesis, II. General mechanisms // J. Sedimentary Petrology. 1985. Vol. 55. No 3. P. 312-321.

Balitsky V.S.[1], Balitskaya E.D.[1], Bublikova T.M.[1], Golunova M.A.[1], Setkova T.V.[1], Balitskaya L.V.[1], Plotnikova I.N.[2], Petrov S.M.[3], Lakhova A.I.[3] Experimental study of the real sources of liquid and gas hydrocarbons at the replacement of reserves of oil and gas deposits. UDC: 549.743.1:546.06

[1] IEM RAS, Chernogolovka (_balvlad@iem.ac.ru_) [2] IAI TAS, Kazan [3] KNRTU, Kazan

Abstract. The article is devoted to the phenomena of replenishment of depleted during the operation of oil and gas deposits. Deposits of Tatarstan are good example in this regard. It has been unequivocally established that the renewal of liquid and gas hydrocarbon (HC) reserves in them occurs constantly, causing a discussion about where and how new portions of oil and gas flow. We solved these issues based on in situ study of synthetic hydrocarbon inclusions in quartz grown in the same experiments in which oil and bituminous rocks were interacted with hydrothermal solutions at temperatures of 240–550 °C and pressures of 5–150 MPa. As a result, it has been established that the real sources of new portions of oil and gas can be liquid and gas hydrocarbons generated by the interaction of the above rocks with hydrothermal solutions, especially those in a homogeneous supercritical state.

It is known that hydrothermal solutions in the earth's interior usually contact and interact with crude oil. The nature of such interactions at elevated and high temperatures and pressures has not yet been sufficiently studied. This is especially important for the phase composition and states of oil located at depths of more than 5–10 km at temperatures of 150–290 °C and pressures of tens of megapascals. A further increase in depths and, along with it, thermobaric parameters in the search, exploration and production of oil further complicates forecasts regarding its phase composition and especially states. It is also obvious that without these data it is impossible to solve a number of questions of the genesis of oil and its secondary replenishment in depleted deposits. Experimental studies based on the visualization of the processes occurring during heating and cooling of synthetic water-hydrocarbon inclusions in quartz grown simultaneously with the interaction of oil with hydrothermal, including sub- and supercritical solutions at temperatures 240 - 550 °C (single experiments - up to 700 °C) and saturated steam pressures and higher (up to 150 MPa) has prospect. The advantage of the chosen approach is the possibility of direct (in situ) determination of both the phase composition and the states of water-oil systems at elevated and high temperatures and pressures. The study of fluid inclusions was carried out using the methods of modern thermobarogeochemistry (Ermakov, Dolgov, 1979; Redder, 1987). The most informative among them were microthermometry, conventional and fluorescence microscopy, local, including high-temperature (up to 400 °C) IR and Raman spectroscopy, as well as gas-liquid chromatography (Balitsky et al., 2005; Balitsky et al. 2016).

The experiments were carried out with crude oil and bituminous rocks of the Bavlinskoye field (Tatarstan). Oil and rocks were subjected to heat treatment in autoclaves with a volume of 30 to 280 ml, made of heat-resistant stainless steel and Cr–Ni alloy. Autoclaves were heated in shaft electric furnaces. Temperature control and regulation was carried out using standard thermometers (TYP 01 T4, TYP R3, Thermodat-25M1). The temperature measurement accuracy was ±3ºC. The autoclaves were first loaded with quartz charge and seed ZY- and ZX-plates 2–4 mm thick, 4–8 mm wide, and 140–200 mm long; then they were filled with one of the initial aqueous solutions (3, 5, and 10 wt. 0.5, 2, and 4 wt % Na_2CO_3) and then crude oil. The required pressure was set by the filling factors of the solutions. The volume of filled oil was changed from tenths to 70–85 volume % with respect to the volume of the filled aqueous solution. The duration of the experiments was mainly 20–30 days, but in a number of control experiments it decreased to several days or, conversely, increased to 100–200 days. The preparation of equipment and materials for the experiments was discussed in detail in our earlier publications (Balitsky et al., 2004; Balitsky et al. 2016). Examples of synthetic water-hydrocarbon inclusions in quartz crystals are shown in photographs (Fig. 1), and the main results on the phase composition and states of inclusions at elevated and high temperatures and pressures are shown on microthermograms (Fig. 2 - 4). It should be noted that microthermograms were compiled on the basis of video films shot in automatic mode in special high-temperature chambers.

Interesting and unexpected result was obtained after repeated autoclave heat treatment of the inclusions for 15 days at different temperatures. After treatment at 300°C, the phase composition and volume ratios of the phases in the inclusions remain unchanged. However, at 320 °C, methane, CO_2, and residual solid bitumen appear in them. The proportion of light fractions also increases. An increase in temperature to 350 and 380°C leads to the gradual disappearance of liquid hydrocarbons and the aqueous phase with a simultaneous increase in the proportion of methane, carbon dioxide, and solid bitumen. This is clearly seen in the inclusions (Fig. 5). Moreover, in experiments at temperatures of 450–500 °C and a pressure of 100–120 MPa, in such inclusions, liquid hydrocarbons completely disappear with their transformation into solid bitumen and methane, and at 670 °C , according to the Raman spectra, solid bitumens give way to crystalline graphite.
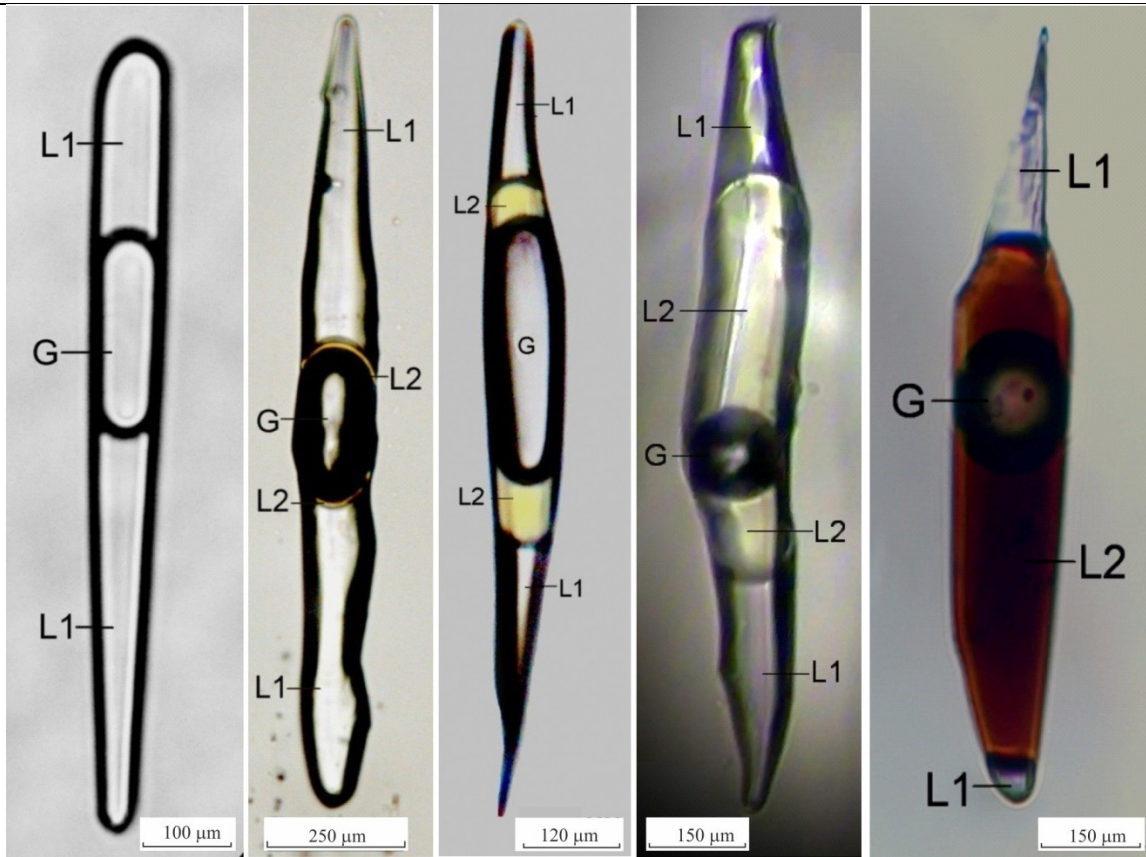
Fig. 1. Examples of quartz crystals with water-hydrocarbon inclusions, grown in the temperature range of 240 – 670 °C and pressures of 5 – 150 MPa in alkaline and weakly alkaline solutions in the presence of bituminous rocks and crude oil. Symbols: L1 - aqueous solution, L2 - liquid hydrocarbons (oil), G - gas hydrocarbons, mainly methane.
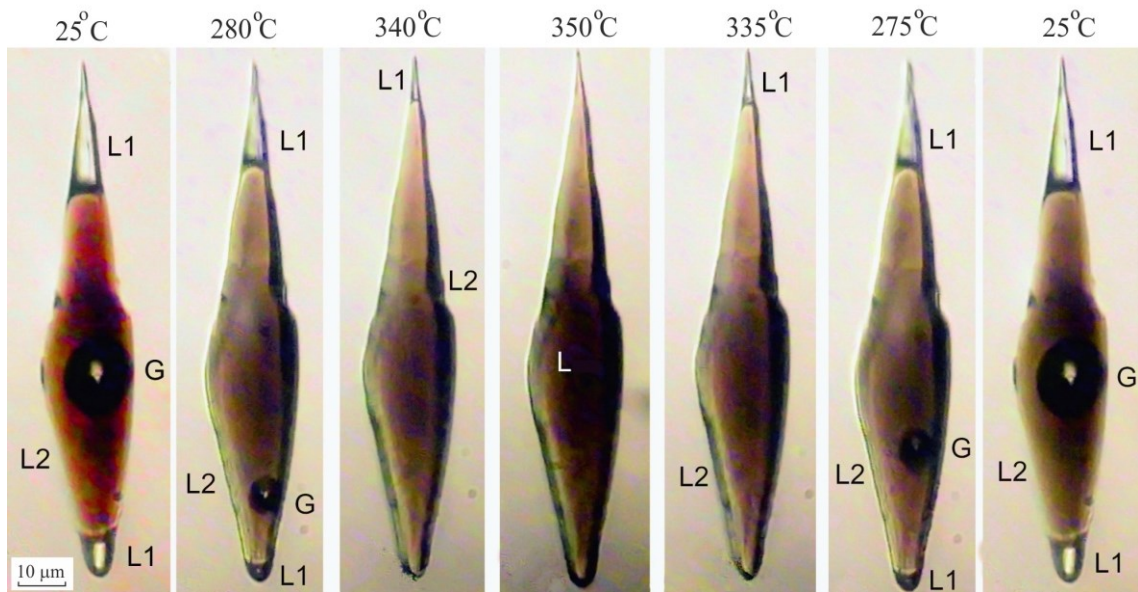

Fig. 2. The thermogram of predominantly oil inclusions shows reversible processes of sequential dissolution of the L3 phase (composition not yet installed) in the bulk of liquid hydrocarbons (L2), then dissolution of the gas bubble in the L2 phase and complete dissolution in the L2 phase of the aqueous phase and then transition of the fluid to the homogeneous state. As the temperature decreases, fluid heterogenization occurs with the sequential appearance of all previously dissolved phases.
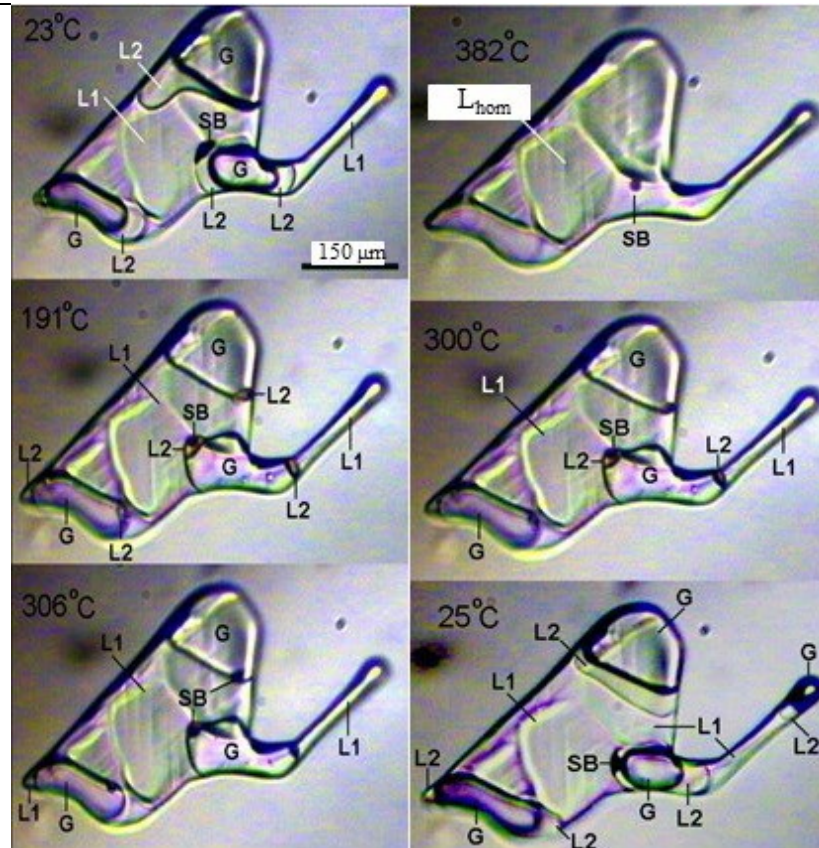
Fig. 3 Reversible change in the phase composition and state of a high-temperature water-hydrocarbon inclusion in the temperature range 23 °C - 382 °C - 25 °C. Volume ratio of phases under normal conditions L1>G≈L2>>SB. The proportion of the solid bitumen (SB) phase remains virtually unchanged over the entire temperature range. Liquid hydrocarbons are completely dissolved as the inclusion is heated to 306 °C with its transition to a two-phase gas-liquid (L1≈G) state. At 382°C, the gas (mainly methane) phase disappears with the transition of the inclusion to a homogeneous state. Cooling the inclusion completely returns it to the original phase compositions and states. Inclusion formation condition: 5 wt. % NaHCO$_3$ +10 vol. % oil, temperature 305/405 ºC, pressure ~70 MPa, duration 14 days.
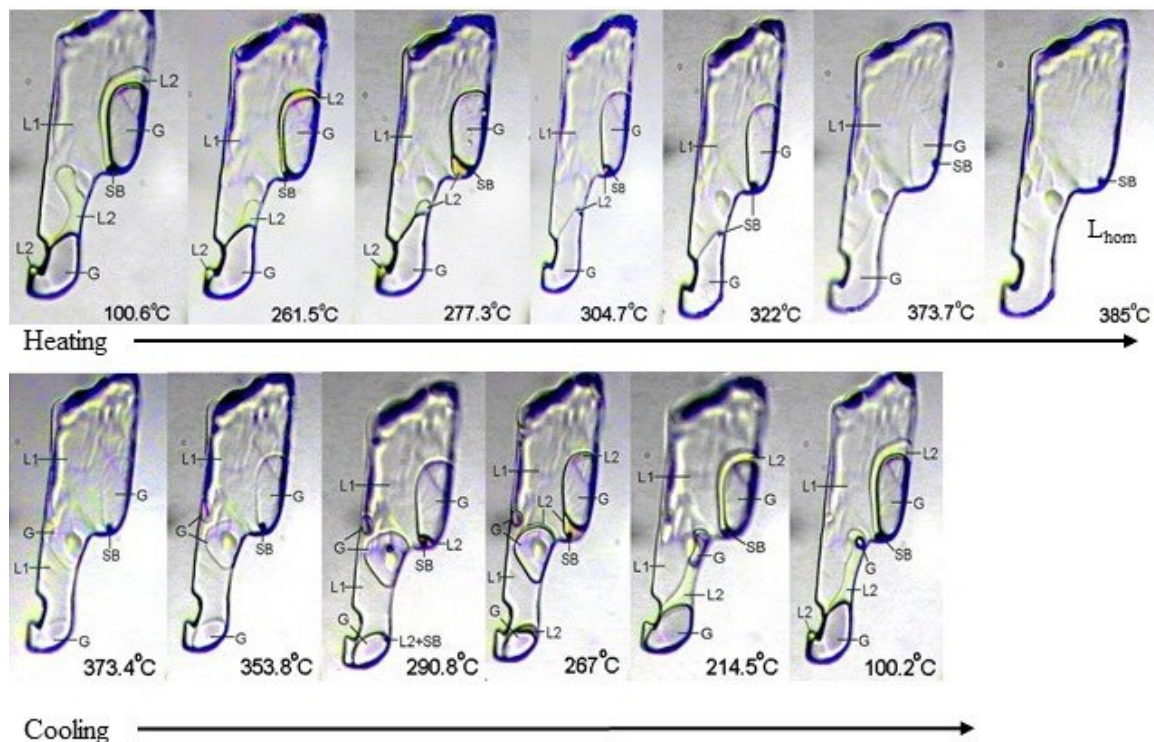

Fig. 4. Changes in the phase composition and state of a high-temperature water-hydrocarbon inclusion with a volume ratio of phases L1>G>L2>>SB during heating and cooling. The solid bitumen (SB) phase remains practically unchanged over the entire temperature range. Below 100 ºC, the changes are insignificant and up to 322 °C, the inclusion retains a

three-phase (taking into account the SB phase - four-phase) state. At 322°C, the phase of liquid hydrocarbons disappears (dissolves), and the fluid passes into a two-phase gas-liquid state. A further increase in temperature to 385°C leads to complete homogenization of the fluid with the disappearance of the gas (mainly methane) phase. Inclusion formation condition: 10 wt. % $NaHCO_3$, temperature 385/405 °C, pressure 120 MPa, duration 20 days.
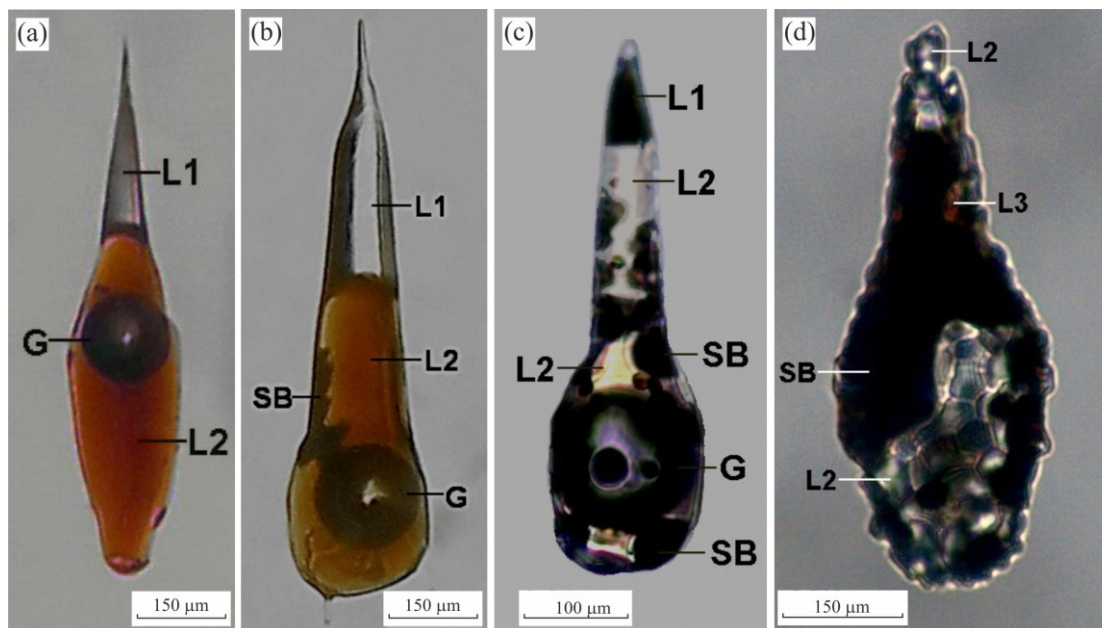

Fig. 5. Predominantly oil water-hydrocarbon inclusion after autoclave treatment at (a) – 300 °C, (b) – 320 °C, (c) – 350 °C, (d) – 380 °C and 100 MPa for 14 days. Up to 300 °C, no changes are observed in water-hydrocarbon fluids. At 320 ºC and above, solid bitumen (SB) appears in them, the proportions of methane, CO2 and light liquid hydrocarbons (L2) increase, reaching a maximum at 350 ºC; above 380°C, liquid hydrocarbons almost completely disappear, turning into solid bitumen, gaseous hydrocarbons, and CO_2. Conditions for the formation of inclusions: aqueous solution of 7.5 wt. % Na2CO3 + 10 vol. % oil, temperature 280/310 °C, pressure 12 MPa.

Thus, the analysis of microthermograms with the determination of the phase composition and states of trapped inclusions convincingly proves the existence of various types of water-hydrocarbon fluids in the earth's interior. The main ones are:

– heterogeneous three-phase fluids with volumetric phase ratios: L1>G>>L2;

– heterogeneous two-phase liquid aqueous-hydrocarbon fluids with a phase ratio L2>>L1 with a completely dissolved gas phase G;

– homogeneous liquid predominantly aqueous fluids $L1_{hom}$ with completely dissolved gaseous and liquid hydrocarbons;

– homogeneous gas fluids G_{hom} with completely dissolved phases of liquid hydrocarbons and water;

– homogeneous hydrocarbon fluids $L2_{hom}$ with completely dissolved aqueous (L1) and gas (G) phases.

References

Balitsky V.S., Balitskaya L.V., Bublikova T.M., Borkov F.P. Water-hydrocarbon inclusions in synthetic quarts, calcite, and fluorite crystals grown from oil-bearing hydrothermal solutions (experimental data)// Doklady Earth Sciences. 2005. Vol. 404. No7. P.1050–1053.

Balitsky V.S., Penteley S.V., Pironon J., Barres O., Balitskaya L.V., Setkova T.V. Phase states of hydrous–hydrocarbon fluids at elevated and high temperatures and pressures: Study of the forms and maximal depths of oil occurrence in the earth's interior// Doklady Earth Sciences. 2016. Vol. 466 No 2. P.130–134.

Ermakov N.P., Dolgov Yu.A. Thermobarogeochemistry. Publishing House Nedra, M.1979, 271 p. (in russian).

Redder E. Fluid inclusions. The nature of inclusions and methods for their study. Volume 1. M.: Mir, 1987. 560 p. (in russian)

Kotelnikov A.R.[1], Damdinov B.B.[2], Suk N.I.[1], Damdinova L.B.[2], Kotelnikova Z.A.[1,3], Akhmedzhanova G.M.[1] Transport of matter under the Earth's crust conditions and the genesis of ore deposits (experimental studies). UDC: 553.21/.24

[1]IEM RAS, Chernogolovka Moscow district, (kotelnik@iem.ac.ru); GI SB RAS, Ulan-Ude (**damdinov@mail.ru**); [3]IGPMG RAS, Moscow (kotelnik@igem.ru)

Abstract. Model experiments have been carried out to study the transport of matter under the conditions of the lithosphere. The experiments were carried out at T=500-680°C and a pressure of 1.5-5 kbar in concentrated water-salt solutions under a temperature gradient in a high gas pressure vessel. The temperature gradient in the experiments was 0.5°C/mm, the duration of the experiments was 14 days. It is shown that intensive recrystallization and precipitation of sulfide minerals (sphalerite, galena, chalcopyrite, pyrite, cooperite, etc.) occur at a temperature of 680-650°C together with feldspars, micas and quartz. The data obtained make it possible to explain the Krauskopf paradox and show the possibility of quantitative modeling of ore genesis processes.

Keywords: experiment, ore genesis, water-salt solutions, sulfide minerals

To understand the mechanism of transport of ore matter under the conditions of the earth's crust, it is necessary to study the chemical and phase composition of fluids in the presence of silicate matter. The main problems of transport and ore deposition are as follows.

(1) What is the source of the ore substance, what processes lead to the concentration of ore elements.

(2) Conditions for the transport of matter – at what temperatures and pressures is the transport of matter carried out in the conditions of the earth's crust? What is the phase and chemical composition of the transport fluids? The role of fluid heterogenization in the transfer of matter.

(3) Krauskopf's paradox – many deposits were formed in post-magmatic (hydrothermal) conditions, however, the solubility of ore elements in water-salt solutions is low and volumes of solutions are required by 3-5 orders of magnitude greater in mass than the mass of ore. Then we should see signs of hydrothermal reworking of host rocks. Where are the traces of these metasomatic processes?

(4) Nests of ore minerals occur in quartz veins (polymetal sulfides of Sadon, Caucasus); the famous "apogranites" of Transbaikalia – with accumulations of tantalum-niobate crystals in altered granites. According to a number of features (study of fluid inclusions), both ores and host rocks are syngenetic. How did they form at the same time? What solutions are needed so that they simultaneously transport both the silicate substance and ore components?

(5) Albitization, K-feldspathization, silicification – its mechanism, significance and role in the formation of ore deposits.

The answer to the first question may be the preliminary concentration of the ore substance in the process of differentiation of silicate melts. In the process of crystallization 1, incompatible elements enrich the residual melt, or in the form of a high-density liquidus crystalline phase, being precipitated, are separated from the silicate melt (chromites). A very important mechanism for concentrating ore matter is liquid immiscibility: (1) separation of sulfide droplets from the silicate melt; (2) layering of the silicate melt in the presence of fluid into two liquids, with enrichment of one of the phases in ore elements; (3) layering of the silicate melt - salt melt type, etc. The primary accumulation of sulfide minerals may be submarine deposits of "black smokers".

The conditions of substance transfer require an accurate assessment of the TP-parameters of the processes, for which we have a complex of mineral thermometers and barometers that allow us to estimate the parameters with an accuracy of ±30°C and ±0.5 ÷ 1 kbar. To assess the compositions of ore-forming fluids, studies of the compositions of fluid inclusions are widely used. It can be concluded that the following salt composition (per 100% dry salt) of ore fluids is: (NaCl+KCl) ~ 40-50 wt%, (Na$_2$CO$_3$+K$_2$CO$_3$) ~ 30-40 wt%, NH$_4$Cl ~ 10 wt%. In some cases (alkaline magmatic rocks, lithium-fluorine granites), fluorides (NaF+KF) begin to play an important role in the composition of fluid salts. The presence of carbon dioxide is almost always noted. The phase composition of the fluid is determined by the PTX-parameters. The salt load of the ore-bearing fluid is (on average) 15÷50 wt%. Fluid heterogenization by the salt hydrolysis reaction NaCl + H$_2$O = NaOH + HCl produces acidic and alkaline components. This reaction in a homogeneous fluid is reversible; in the presence of a two-phase system, an interphase redistribution of alkaline and acidic components occurs: acids enrich the less dense phase, and alkalis enrich the denser one. This mechanism of reactions in heterophase systems allowed D.S. Korzhinsky put forward the position on the waves of acidic and alkaline fluids. Moreover, the later, alkaline fluid was considered ore-bearing. Therefore, we set the task of studying the transport of matter in the ore (alkaline) phase of the fluid.

To overcome the "Krauskopf paradox", sufficiently high concentrations of ore metals in the mineral-forming fluid are required. In addition, such a fluid must simultaneously transport both silicate and ore matter.

Experiments to study the transport of ore matter were carried out at a temperature of 500–650°C and a pressure of 3–5 kbar. It is these values of PT-parameters that were obtained for a number of deposits using mineral thermometers and barometers and the results of studying fluid inclusions. The total salt concentration in the model fluid was 37–41 wt%. The experiments were carried out in the temperature gradient mode of 30-40°C. All experiments were performed using the ampoule method in high gas

pressure vessel designed by IEM RAS. The accuracy of temperature regulation and control was no worse than ±2°C, pressure ±50 bar. Gold and platinum ampoules 7 mm in diameter and 70 mm long were used. The duration of the experiments was 14 days. The initial sample was placed in the lower part of the ampoule and transported to the upper part. Table 1 shows the conditions of experiments on the transport of marine sediment material (basalts and black smokers), in order to simulate the formation of the Zun-Kholbinsk polymetal and gold deposit.

Experiments 7368 and 7369 are characterized by the formation of parageneses of the Fsp + Qz + sulfides type in the upper part of the ampullae (Fig. 1a).

We have carried out experiments on the joint transfer of a number of ore elements Fe, Ni, Cu, Zn, As, Cd, Hg, Bi, Au under gradient conditions at a temperature T_{bottom}=680°C; T_{top}=650°C; P=5 kbar, with the duration of the experiment 14 days. Loading of gold ampoule with a diameter of 7 mm is shown in table 2.

As a result of the experiment, it was shown that a number of elements form their own minerals, while others are present in the form of isomorphic elements: Fe, Ni, Cu are included in pyrite, pyrrhotite; Pb, Au, As, Bi, Zn are present in galena; sphalerite includes Zn, Cd, Fe, Mn, Cu; As is included in galena, orpiment, realgar, gold; Hg is present in gold. Figure 1b shows intergrowths of minerals from run 7387. Thus, it is shown that ore and silicate matter can be transported together by a relatively simple fluid and form ore parageneses.

Table 1. Experiments on the transport of substances from submarine marine sediments (T_{bottom}=680°C; T_{top}=650°C; P=4 kbar; experiment duration 14 days).

№ sample	Weight, mg	Salts, mg	H_2O, μl	Experience Products
7368	184 powder VTP bas[1)], 111 ZnS+176 BS +135Qz(gl)+202Ab+284 Qz	50 NH_4Cl + 100 NaCl + 100 Na_2CO_3	460	Ab +Cpx+ Qz + ZnS + PtS
7369	150 powder VTP bas, 100 ZnS+200 BS +100Qz(gl)+10 FeO+10 grp+ 100Mic+243 Qz	200 K_2CO_3 + 200 KCl + 100 NH_4Cl	720	Ksp+Qz+ZnS+PbS+ PtS+ $CuFeS_2$

1) powder VTP – basalt, BS – black smoker substance (base ZnS+ a little PbS); Qz – quartz, Qz(gl) – quartz glass; Ab – albite, grp – graphite, Cpx – clinopyroxene; Ksp – potassium feldspar.
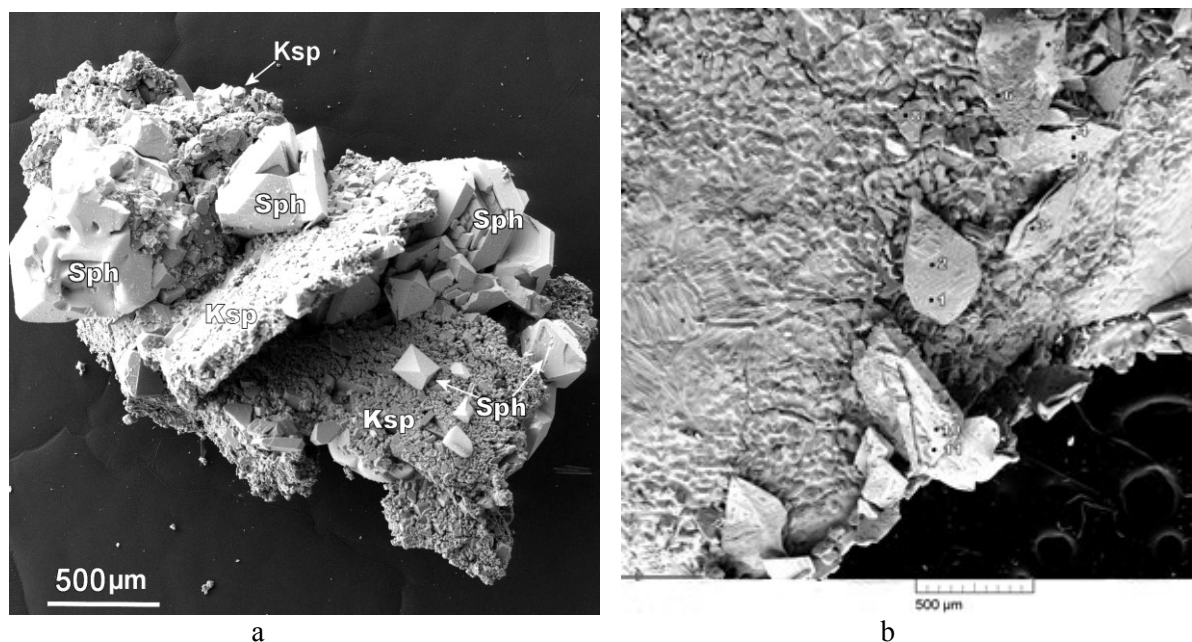

Fig. 1. Paragenesis of Ksp + Sph (experiment 7369) – a; 1,2 – orpiment; 3.5 – realgar?; 4.7 – Au (with As, Hg); 6 – Sph (with Mn, Fe, Cd, Cu, As); 8 – (PbS+As_2S_3); 9, 10 – Gn (with As, Cd). Ksp – potassium feldspar, Sph – sphalerite, Gn – galena – b.

Table 2. Experiment in the joint transport of ore elements

№ sample	Weight, mg	Solution, salts, mg	H_2O, μl	Products of experience (top of the ampoule)
7387	260 powder VTP bas[1)], + 210 BS+ 72 CPy+ 44 Pentl + 14 AsPy+ 24 CdS + 10 HgS +10 Bi_2O_3+28 Au +135 Qz(gl)+202 Ab +284 Qz	120 NH_4Cl+ 50 NaCl+90 Na_2CO_3 + 100 μl 20% NaOH + 20 C + 20 S	360	Qz + Ab + Cpx + Sph + Py + Pyr + Wrz + Gn +_orpiment + realgar + Au

1) powder VTP – basalt, BS – black smoker substance (base ZnS+ a little PbS); Qz – quartz, Qz(gl) – quartz glass; Ab – albite, grp – graphite, Cpx – clinopyroxene; AsPy – arsenopyrite; Cpy – chalcopyrite; Gn – galena; Py – pyrite; Pyr – pyrrhotite; Wrz – wurtzite; Sph – sphalerite.

Table 3. Experiments on the transport of tantalite under gradient conditions: T_{bottom}=700℃; T_{top}=650℃; pressure 3.5 kbar. The duration of the experiments was 14 days.

№ sample	Weight, (bottom of ampule)	Solution	Total salinity	Experience Products
7399	Tnt +Fsp+ Qz	NaF+NaCl+Na_2CO_3+NH_4Cl	25 wt%	Tnt+ Ab +Qz+gl
7400	Tnt +Fsp +Qz	KF+KCl+K_2CO_3+NH_4Cl	31 wt%	TnT+Mcl+Ksp+Rip+Qz+gl

1) mineral indices: Ab – albite; Fsp – alkaline feldspar; gl – silicate glass; Ksp – potassium feldspar; Mcl – microlite; Qz – quartz, Rip – rippit; Tnt – tantalite.

Experiments were carried out to study the transport of tantalite together with a silicate substance. These experiments were carried out in order to test the hypothesis of a possible hydrothermal origin of ore apogranites in Transbaikalia. For the Orlovsky deposit, the TP-parameters for the formation of apogranites were determined: temperature is about 600-650℃, pressure is ~3.5 kbar. These parameters were estimated for the formation of Orlovka apogranites from the structural state of feldspars and from the study of the densities of carbon dioxide in fluid inclusions. The conditions for conducting experiments on the transfer of tantalite and silicates are given in Table 3. Figure 2 shows parageneses of tantalite with silicate minerals of the experimental products.

Based on our experiments, we can conclude that it is possible to transport and concentrate the substance of tantalum-niobate ores at the hydrothermal, post-magmatic stage of the evolution of lithium-fluoric granites. Most likely, this mechanism could be implemented during the formation of ore apogranites in Transbaikalia.

Conclusions

It is shown that ore components are able to migrate at relatively high parameters due to concentrated water-salt fluids. Mineralizers are solutions of chlorides, alkali metal carbonates and ammonium salts. In some cases, alkali metal fluorides may be present in the salt composition. These model solutions are distinguished by increased alkalinity and can serve as a model for solutions of the alkaline ore stage of mineral genesis (according to D.S. Korzhinsky).
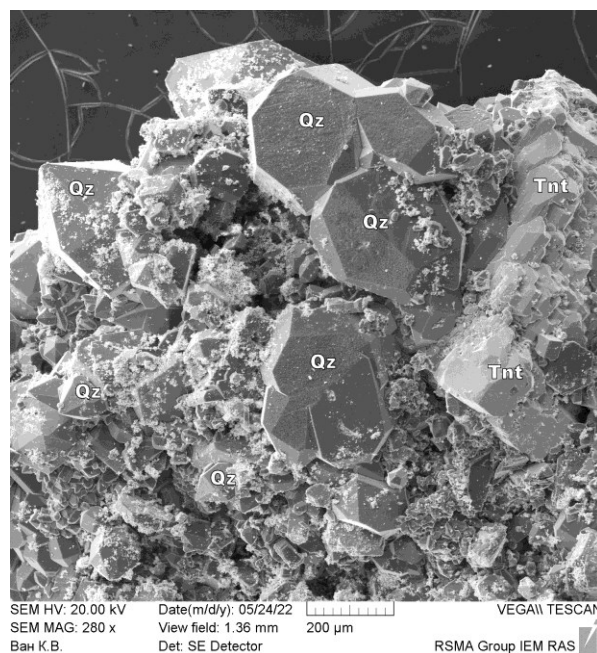

Fig. 2. Crystals formed as a result of the transfer of a substance to the upper part of the ampoule. Qz – quartz, Tnt – tantalite.

Along with the ore components, a silicate substance is transported in water-salt solutions, which gives to these water-salt systems the properties of II (P-Q) type solutions, characterized by a number of features: high solubility of both silicate and ore minerals, the presence of a lower (liquid-vapor) and the upper (liquid1-liquid2) regions of heterogenization, where separation into two fluids

occurs – a highly concentrated brine and a weakly concentrated aqueous fluid.

The deposition of ore components occurs mainly from highly concentrated fluids, later they are displaced by weakly concentrated fluids. The latter are conserved as fluid inclusions containing low concentrations of ore elements. Nevertheless, when analyzing the FI of quartz from ore parageneses, inclusions with anomalously high concentrations of metals are encountered. Apparently, they are relics of highly concentrated – ore-forming solutions.

Kotova N.P. Experimental study of Nb_2O_5 solubility in KF solutions at 550° C and from 50 to 500 MPa.

Institute of Experimental Mineralogy RAS, Chernogolovka Moscow district kotova@iem.ac.ru

Abstract. Experimental data on the niobium oxide solubility in KF solutions with a concentration of 0.1 and 1.0 m at 550° C and 50, 100, 200 and 500 MPa were obtained. It was found that with an increase in pressure from 50 to 200 MPa, the Nb content in 0.1 mKF solutions increases by an order of magnitude. With a further increase in pressure to 500 MPa, the niobium content practically does not change and remains in the range of $10^{-2.5}$ mol / kg H_2O.

Keywords: experiment, oxide niobium, hydrothermal solubility, pressure, fluoride solutions

For many years, we have been conducting systematic experimental and field geological studies aimed at obtaining quantitative estimates of the physico-chemical conditions for the formation of greisen and albitite deposits of W, Mo, Sn, Ta, Nb and Li associated with standard lime-alkaline, including lithium-fluoride granites. Despite the great achievements of geologists in the field of studying ore-bearing granites and related greisen, albitite and other genetic types of rare metal deposits, many fundamental questions of their genesis still remain unclear. As is known, there are various hypotheses of the genesis of these deposits - magmatic and hydrothermal-metasomatic.

The most generally accepted are the genetic concepts of V.I. Kovalenko [Kovalenko, 1977], consisting in the fact that rare-metal lithium-fluoride granites containing tantalum ores are formed as a result of crystallization fractionation of ordinary granite magma under specific conditions that ensure the gradual accumulation of F, Li, Ta, Nb and other rare metals in the residual granite melt.

However, to model the conditions for the formation of tantalum deposits, it is also necessary to take into account the role of hydrothermal-metasomatic processes [Beus et al., 1962]. The results of our experimental studies under conditions of temperatures, pressures and compositions of solutions corresponding to the physicochemical parameters of postmagmatic processes may provide some new criteria and limitations regarding the interpretation of geological data and the assessment of the degree of reliability of a particular genetic hypothesis of the origin of rare-metal deposits in granites.

New experimental data were obtained on the solubility of niobium oxide (β- Nb_2O_5), an analogue of the mineral nioboxide, rarely found in nature, in 0.1 and 1 m KF solutions at 550 °C and 50, 100, 200 and 500 MPa. The run duration was 10 - 18 days. Experiments at 550 ° C and 50 to 100 MPa were performed on a hydrothermal line. A sealed-capsule quench technique was employed.

Experiments at 550°C and 200 to 500 MPa were carried out on a high gas pressure installation with internal heating (gas bomb). It allows reaching pressures up to 6 MPa and temperatures up to 1400 ° C. Run temperatures were measured with an accuracy of ± 5 °C. The pressure was regulated with a maximum uncertainty of ± 5 MPa. Regulation and maintenance of the required temperature in the working chamber of the furnace is carried out using the TRM-101 OVEN thermostat through two S-type thermocouples (Pt90Rh10-PT100). Thermocouples are mounted at the top and close to the bottom of the chamber to control the temperature gradient. The chamber system pressure is set from above by pure argon gas pressure. The lid of the working chamber is made of pyrophyllite. Aluminum oxide and kaolin wool serve as filler in the chamber with ampoules.

The quenched aqueous solutions were then analyzed using ICP/MS (Inductively Coupled Plasma Mass Spectrometry) and ICP/AES (Atomic Emission Spectroscopy) for Nb, Ta, Mn, and Fe and admixture elements Ti, W, and Sn,.

To control congruent or incongruent dissolution of Nb oxide and to determine chemical composition of newly-formed phases (in case of their detection) the initial materials and solid run products were studied by X-ray diffraction, and electron microprobe analysis (Cam Scan MV 2300 (VEGA TS5130MM).

The experimental results are shown in Figures 1 and 2. Analysis of the data obtained showed that in 0.1 m KF solutions, an increase in fluid pressure from 50 to 200 MPa leads to an increase in the solubility of niobium oxide by one order of magnitude (from $n*10^{-3.5}$ to $n*10^{-2.5}$ m). With a further increase in pressure from 200 to 500 MPa, the solubility of niobium oxide does not change, remaining at the level of $n*10^{-2.5}$ m. With an increase in the concentration of F^- - ion (1 m KF solutions), the equilibrium content of Nb increases, reaching a significant value ($n*10^{-2}$ m.). However, in concentrated 1 m KF solutions, with an increase in

fluid pressure from 50 to 500 MPa, the solubility of Nb_2O_5 practically does not change, remaining at the level of n *10^{-2} m.

Comparison of the experimental results on the solubility of niobium oxide in KF solutions at T = 550° C and a pressure of 50 and 100 MPa [Kotova, 2012; Kotova, 2014] showed that the trends of the dependence of the solubility of niobium oxide on the concentration of the F-ion are very close (Fig. 2). However, lowering the fluid pressure from 100 to 50 MPa in 0.01 m solutions of KF leads to a decrease in the solubility of Nb_2O_5 by about one order of magnitude, and in 0.1 m solutions of KF – by 0.5 orders of magnitude. With a further increase in the concentration of KF, the effect of lowering the fluid pressure ceases to affect the solubility of Nb_2O_5. Starting from a concentration of 0.3 m KF, the niobium content in the solution has similar values both at P = 100 MPa and at P = 50 MPa, reaching a value of 10-1.5 m in a solution of 2 m KF, quite sufficient for real mass transfer of niobium by hydrothermal solutions.
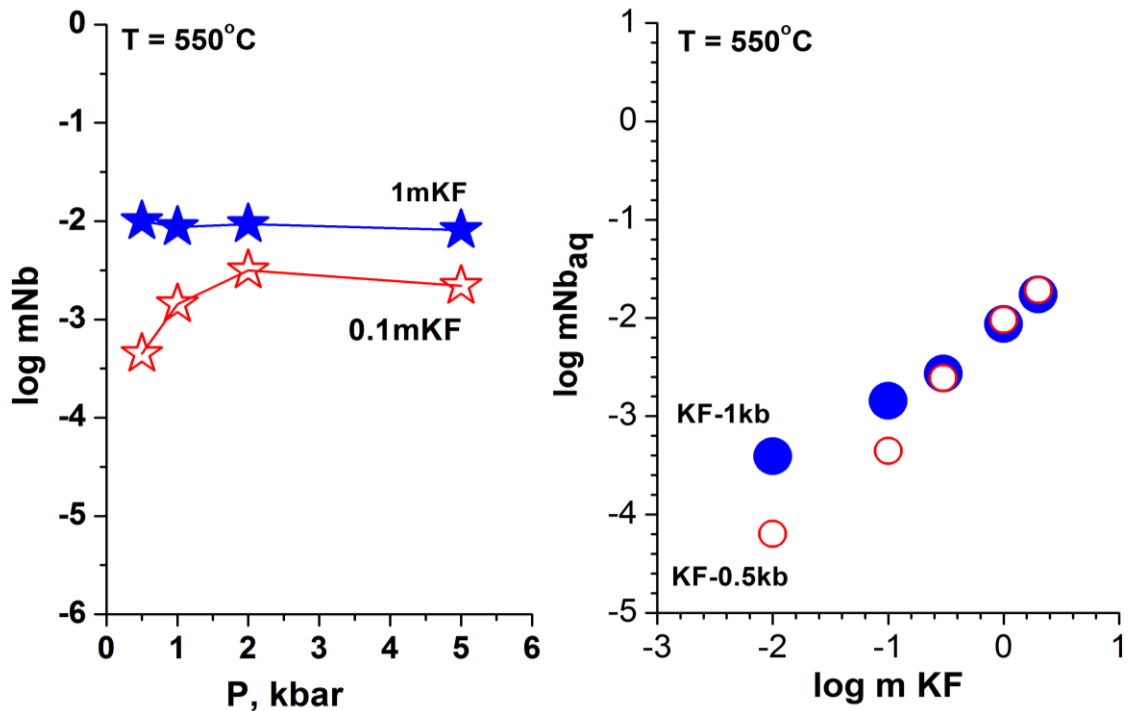

Fig.1. Influence of KF concentration and fluid pressure on the Nb_2O_5 solubility at T = 550° C (asterisks – 0.1 m KF, shaded asterisks - 1 m KF)

Fig.2. Influence of KF concentration and fluid pressure on the Nb_2O_5 solubility at T = 550° C (circles–at P = 0.5kb, shaded circles–at P=1kb)

The results of the X-ray phase method of analysis of solid products of experiments showed that niobium oxide dissolves congruently in 0.01 m KF solution. In KF solutions of higher concentration, niobium oxide dissolves incongruently. At the same time, in 0.1 m solution of KF, niobium oxide is replaced with potassium oxifluoride of the $KNb_6O_{15}F$ type, belonging to the monoclinic syngony, and in 0.3, 1 and 2 m solutions of KF, crystals of potassium niobate $K_2Nb_4O_{11}$, belonging to the tetragonal syngony, are formed.

The experimental results obtained by us can serve as an objective basis for assessing the possibility of mass transfer of niobium by hydrothermal solutions under natural conditions, since based on the type of concentration curves obtained, it is possible to judge the maximum possible concentration of Nb in an aqueous fluid at an early post-magmatic stage after its separation from the crystallizing granite melt. Fundamentally important is the fact that P - T conditions have little effect on the solubility of niobium and tantalum. The solubility of simple oxides (Ta_2O_5 and Nb_2O_5) depends more on the concentration of fluoride fluids

References

1. Beus A.A., Severov E.A., Tisnen F.F., Subbotin K.D. Albitized and greisenized granites (apogranites). Moscow: Publishing House of the USSR Academy of Sciences, 1962.196 p.

2. Kovalenko V.I. Petrology and geochemistry of rare-metal granitoids. Novosibirsk: Nauka SO, 1977, 207 p.
3. Kotova N.P. Experimental study of concentration dependence of niobium oxide solubility in fluoride solutions at T=550 oC, P = 1000 bar and low oxygen fugacity (Co-CoO buffer) Experiments in Geosciences, 2012, V.18, N1, p. 123-125
4. Kotova N.P. Experimental study of Nb2O5 solubility in fluoride solutions at 550oC and 500 bar, Experiments in Geosciences, 2014, V.20, N1, p. 38-39

Lakhova A.I.[1], Petrov C.M.[1], Balitsky V.S.[2], Setkova T.V.[2], Plotnikova I.N.[3], Balitskaya L.V.[2], Golunova M.A.[2], Bublikova T.M.[2] Experimental study of hydrothermal fluid interaction on changes in oil hydrocarbons of different genotypes. UDC: 553.985

[1] KNRTU, Kazan (*lfm59@mail.ru*); [2] IEM RAS, Chernogolovka ; [3] IAI TAS, Kazan

Abstract. We experimental studied of the influence of hydrothermal fluid on oil hydrocarbons of the Volga-Ural oil and gas basin from different depths, related to the geochemical classification of Al.A. Petrov to different genotypes. The experiments with the simultaneous quartz crystal growth at a temperature of 285/307 °C and a pressure of 100 MPa were carried out. As a result, differences in the change in the composition of oil hydrocarbons depending on the genotype when interacting with hydrothermal solutions were established. The content of saturated hydrocarbons in the composition of oil hydrocarbons of type A¹ decreases, and the content of aromatic hydrocarbons and resins increases under hydrothermal interaction. On the other hand, during hydrothermal treatment of oil hydrocarbons of type B², the content of saturated hydrocarbons in their composition increases, the amount of aromatic hydrocarbons decreases, and the content of asphaltenes increases. The composition and volume ratio of phases of fluid inclusions in quartz also depend on the genotype of oil hydrocarbons. All this indicates that the composition of oil hydrocarbons affects the dominance of certain reactions in the hydrothermal fluid.

Keywords: oil hydrocarbons, quartz, synthetic inclusions, hydrothermal fluid, asphaltenes

Supercritical hydrothermal fluids play an important role in the transformation of organic matter, the transfer and redistribution of hydrocarbons in the Earth's shells. Synthetic fluid inclusions in minerals grown simultaneously with the interaction of supercritical fluids with oil hydrocarbons make it possible, using the methods of microthermometry and molecular, especially high-temperature spectroscopy, to trace in situ the change in the phase composition and phase states of liquid and gaseous hydrocarbons and thus characterize their stability and forms of migration, to estimate the maximum depths of being in the earth interior and the stage of thermometamorphic transformations. Fluid inclusions in this case are essentially ultramicrosamples of the reagent medium (vapor and liquid), taken at fixed thermobaric parameters without disturbing the dynamic equilibrium established in the system. In this regard, studies aimed at studying the mechanisms of reactions that describe the transformation of oil hydrocarbons in a supercritical fluid medium seem to be important and relevant.

Oil hydrocarbons of the Volga-Ural oil and gas basin were selected from different depths and different types to identify changes in the composition of oil hydrocarbons depending on the genotype. The first type B² according to the geochemical classification of Al.A. Petrova (Petrov, 1984) is oil hydrocarbons occurring at a depth of 300 m in terrigenous deposits of the Sheshma horizon of the Ufimian stage of the Permian period. The second type A¹ is oil hydrocarbons occurring at a depth of more than 250 m in rocks from anhydrite and carbonates in the deposits of the Artinskian stage of the Permian period (Table 1).

Experiments on the interaction of hydrothermal solutions with oil hydrocarbons, with the simultaneous growth of quartz crystals, were carried out according to a previously developed method (Balitsky et al., 2005, 2016, 2020). Experimental conditions: temperature 285/307 °C, filling factor 80%, solution composition 7.5 wt.% Na_2CO_3, 25% oil, duration 14 days. After the end of the experiments, water-hydrocarbon solutions and inclusions in quartz crystals were all-round studied.

Table 1. Physicochemical properties of oil hydrocarbons of the Ufimian and Artinskian stages

Characteristics	Oil hydrocarbons	
	Ufimian stage	Artinskian stage
Density at 20 ˚C, g/cm³	0.9710	0.9020
Content:		
Sulfur, %	2.8	3.9
Vanadium, mg/kg	400	108
Nickel, mg/kg	100	18

Table 2. Composition of oil hydrocarbons before and after experiments

Component composition, %	Ufimian stage		Artinskian stage	
	before	after	before	after
S	23.53	27.06	60.10	42.14
A	46.95	41.70	25.60	34.74
R	23.31	22.40	8.70	17.59
As	6.21	8.84	5.60	5.53
A/S	1.99	1.54	0.42	0.82
CII*	0.42	0.56	1.91	0.91

S - fraction of saturated hydrocarbons; A - fraction of aromatic hydrocarbons; R - resins; As – asphaltenes; CII* – Index of colloidal instability ((S+As)/(A+R)); A/S is the ratio of aromatic to saturated hydrocarbons;
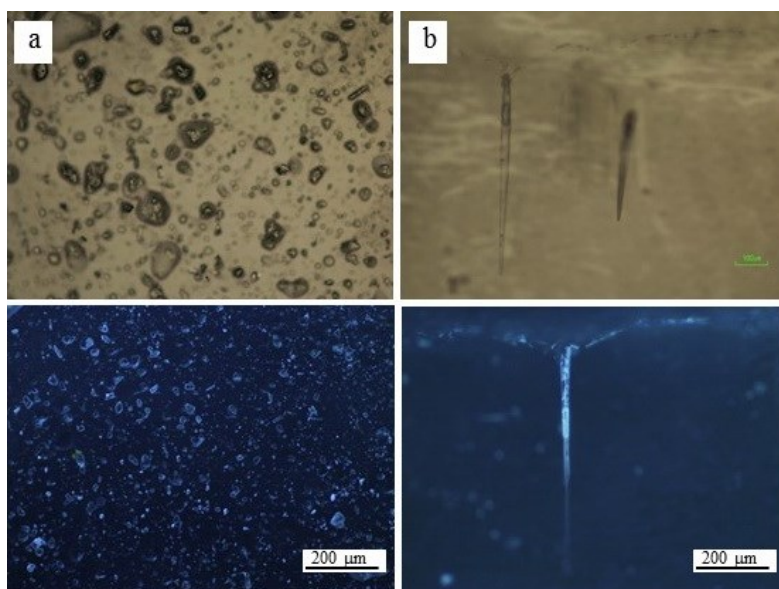

Fig. 1 Micrographs of inclusions in quartz obtained in experiments with oil hydrocarbons of the Ufimian (a) and Artinskian (b) stages. Top image under normal light, bottom under UV light.
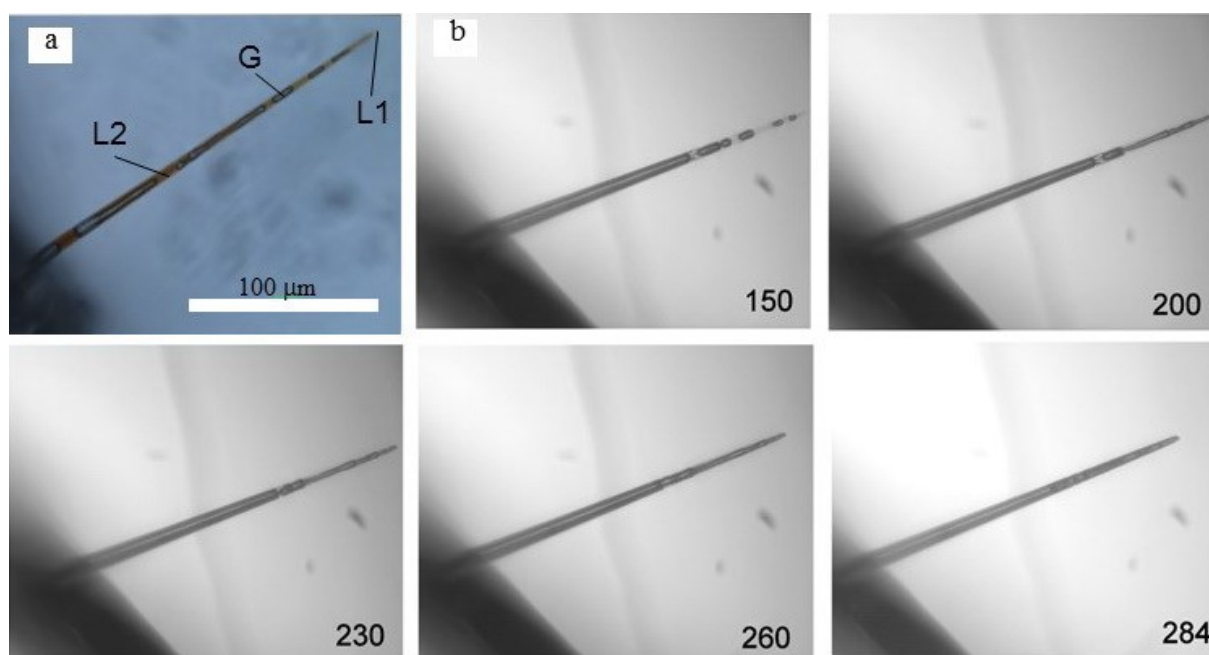

Fig.2 Initial water-hydrocarbon inclusion formed in experiments with oil hydrocarbons of the Ufimian stage (a) and its microthermogram (b). L1 - water solution, G - gas (mainly methane, water vapor and liquid hydrocarbon vapor), L2 - liquid oil hydrocarbons.

Oil hydrocarbons before and after the experiments were separated according to SARA analysis into four fractions: saturated hydrocarbons (S), aromatic hydrocarbons (A), resins (R) and asphaltenes (As). The precipitation of asphaltenes from the extracts was carried out with 40 times the amount of n-hexane. The remaining maltenes were separated by liquid column chromatography using alumina pre-calcined at 425°C. As a result, saturated hydrocarbons eluted with n-hexane, aromatic compounds eluted with toluene, and resins displaced from the adsorbent (Al_2O_3) by a mixture of benzene and isopropyl alcohol in equal proportions were obtained from maltenes.

Microphotographs of water–hydrocarbon inclusions obtained as a result of hydrothermal treatment of oil hydrocarbons of the Artinskian and Ufimian stages differ significantly. For oil hydrocarbons of the Ufimian stage, due to the absence of light fractions, the formation of fluid inclusions in the form of "spheres" is predominantly typical (Fig. 1a). In rare cases, wedge-shaped inclusions are formed, predominantly oil (with a volume ratio of phases L2>L1>G) (Fig. 2a). By comparison the fluid inclusions of the Artinskian stage has wedge-shaped structures, in which phases of an aqueous solution and light hydrocarbons are clearly distinguishable (with the volume ratio of the phases L1>G>L2) (Fig. 1b, Fig. 3a).

The microthermograms of water–hydrocarbon inclusions of both types show a change in their composition and phase state upon heating (Figs. 2b and 3b). Unfortunately, it was not possible to determine the homogenization temperature and trace the behavior of the inclusions during cooling due to their depressurization at 284°C (Ufimian) and 337°C (Artinskian).
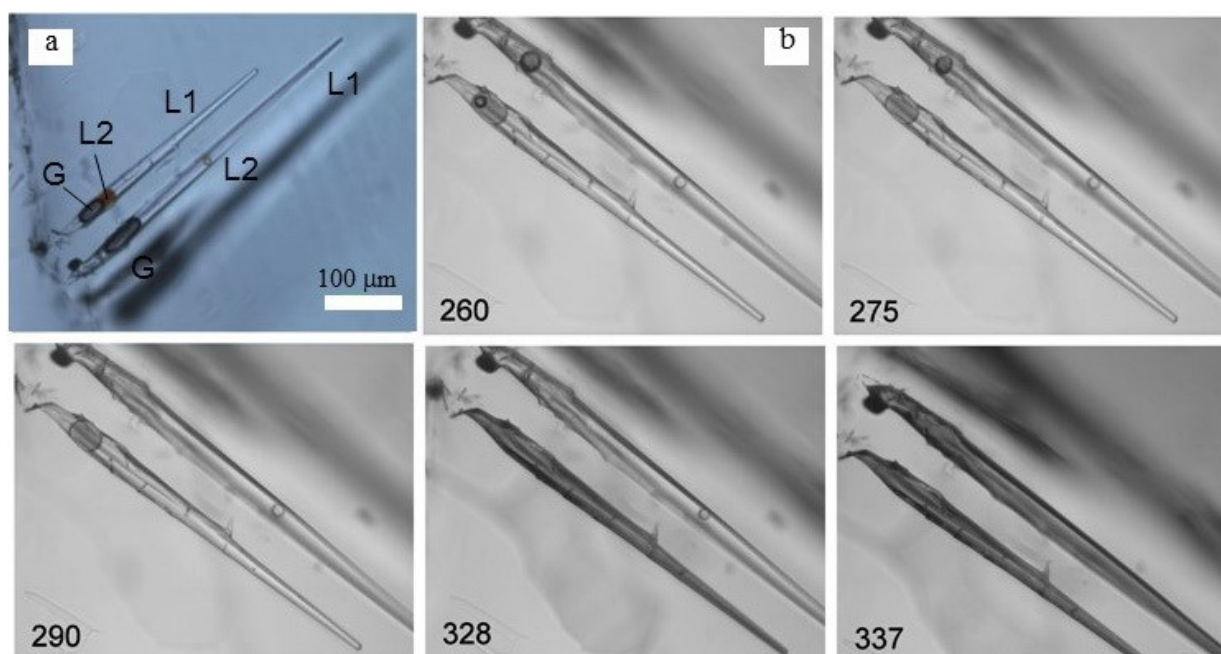

Fig.3 Initial water-hydrocarbon inclusion formed in experiments with oil hydrocarbons of the Artinskian stage (a) and its microthermogram (b).
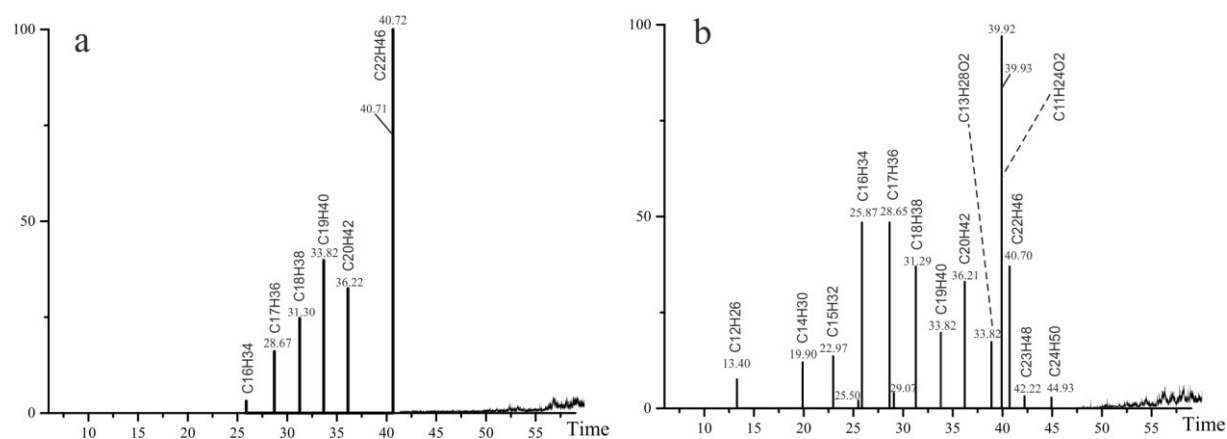

Fig. 4 Chromatograms of the composition of hydrocarbon inclusions obtained as a result of treatment by alkanes m/z=71+85: a) Ufimian stage, b) Artinskian stage.

Markers of n-alkanes C18, C19, C20, C21, C22 were used to identify compounds in the composition of hydrocarbon inclusions (Fig. 4). On the chromatograms of hydrocarbon inclusions in quartz crystals obtained as a result of hydrothermal treatment of oil hydrocarbons of the Ufimian stage with the simultaneous growth of quartz, the presence of alkanes of the linear structure C16, C17 was observed. In hydrocarbon inclusions after hydrothermal impact on oil hydrocarbons of the Artinskian stage, linear alkanes of the composition C12-C17, C24 and oxygen-containing compounds were identified, which may indicate hydrolysis reactions (Fig. 4b).

As a result of the studies, the differences in the change in the composition of oil hydrocarbons depending on their genotype when interacting with a hydrothermal solution were established. Under hydrothermal interaction, the content of saturated hydrocarbons in the composition of oil hydrocarbons of type A^1 decreases, and the content of aromatic hydrocarbons and resins increases. Conversely, during hydrothermal impact on oil hydrocarbons of type B^2, the content of saturated hydrocarbons in their composition increases and the amount of aromatic hydrocarbons decreases, the content of asphaltenes increases. Fluid inclusions in quartz formed in a hydrothermal fluid with oil hydrocarbons of the Ufimian stage are predominantly of oil composition, while inclusions of the Artinskian stage consist mainly of aqueous solution and light hydrocarbons. All this indicates that the composition of oil hydrocarbons affects the dominance of certain reactions in the hydrothermal fluid.

References

Balitsky V.S., Balitskaya L.V., Bublikova T.M., Borkov F.P. Water-hydrocarbon inclusions in synthetic quarts, calcite, and fluorite crystals grown from oil-bearing hydrothermal solutions (experimental data)// Doklady Earth Sciences. 2005. Vol. 404. No7. P.1050–1053.

Balitsky V.S., Penteley S.V., Pironon J., Barres O., Balitskaya L.V., Setkova T.V. Phase states of hydrous–hydrocarbon fluids at elevated and high temperatures and pressures: Study of the forms and maximal depths of oil occurrence in the earth's interior// Doklady Earth Sciences. 2016. Vol. 466 No 2. P.130–134.

Balitsky V.S., Setkova T. V., L. V. Balitskaya, T. M. Bublikova, and M. A. Golunova. Phase composition and states of water-hydrocarbon fluids at elevated and high temperatures and pressures (experiment with the use of synthetic fluid inclusions). In

Advances in Experimental and Genetic Mineralogy, volume 11 of Special Publication to 50th Anniversary of DS Korzhinskii Institute of Experimental Mineralogy of the Russian Academy of Sciences. Litvin Yu.A. Safonov O.G (Editors), New York, 2020. New York.

Petrov Al. A. Oil hydrocarbons. - M.: Nauka, 1984. - 280 p.. (in russian).

Redkin A.F., Kotova N.P. Features of the scheelite interaction with hcl solutions at 400 and 500° C, 100 MPa and various f(O₂) (based on experimental and calculated data).

Institute of Experimental Mineralogy RAS, Chernogolovka Moscow district redkin@iem.ac.ru, kotova@iem.ac.ru

Abstract. Scheelite ($CaWO_4$) dissolves incongruently in HCl solutions in the concentration range from 0.01 to 0.316 m. In dilute solutions containing from 0.01 to 0.0316 mHCl, insignificant amounts of tungsten oxides WO_3 (or) WO_{3-x} are detected in the run products. In solutions containing 0.1 to 0.316mHCl, the formation of calcium tungsten bronzes (CTB) Ca_xWO_3 is observed, the average composition of which corresponds to the formula $Ca_{0.07}WO_3$. An increase in HCl concentration contributes to the WO_3 yield. According to calculations, in a solution containing 0.0316 mHCl, the product yield is 4.8 ± 1.1 mol%, in a solution of 0.1 mHCl – 19.6 ± 6.0, and in 0.316 mHCl – 58.1 ± 15.6. An increase in temperature reduces the WO_3 yield. The analysis of the existing data on the thermodynamic properties of scheelite and tungsten oxides was carried out and calculations were performed in a system simulating the dissolution of scheelite in hydrochloric acid solutions at 400 and 500° C, 100 MPa and $f(O_2)$ in the range from Co-CoO to Cu_2O-CuO buffers.

Keywords: tungsten, calcium, tungsten trioxide, calcium - tungsten bronzes, scheelite, solubility, chloride solutions, thermodynamic calculations

Scheelite $CaWO_4$ (Sch) is the most important ore mineral, which includes the element tungsten, capable of changing its valence during the transition from the solid phase to the solution. Despite a large number of papers devoted to the study of this mineral solubility (Khodakovsky, Mishin, 1971; Forster, 1977; Wood, Samson 2000), the influence of redox conditions on scheelite solubility and the valence state of W in hydrothermal conditions has not been considered.

The aim of our research is to obtain reliable experimental data on the solubility of Sch at parameters close to the conditions of scheelite formation in the Earth's crust, as well as to perform thermodynamic calculations modeling this process, which ultimately will determine the main factors responsible for tungsten accumulation and scheelite deposition in hydrothermal solutions.

The experiments were carried out on a high-pressure hydrothermal apparatus. The capsules with the research material, 0.01, 0.0316, 0.1 and 0.316 mHCl solutions and the container with buffer

were sealed into cold-seal pressure vessel of Tuttle type. Oxygen fugitivity in the reactors was determined by metal-oxide buffer pairs Co/CoO, Ni/NiO and Cu_2O/CuO. As a starting material, scheelite (Sch) was used, obtained by recrystallization of the chemical reagent $CaWO_4$ mark (pure) in $0.1m$HCl at 500° C and 100MPa, for 20 days and subsequent drying at 100° C. The experiments were carried out in platinum ampoules $(0.7 \times 0.2 \times 50$ mm).sealed by electric arc welding. In experiments at 400° C and 100 MPa, 40 mg of scheelite and 0.8 ml of HCl solution were injected into the Pt capsule, and in experiments at 500° C and 100 MPa - 40 mg of scheelite and 0.65 ml of HCl solution.

The analysis of quenching solutions to determine the W and Ca concentration was carried out by the most precise and modern methods of inductively coupled plasma ICP/MS, ICP/AES and AAS.

The phase composition of the solid products was studied by powder X-ray diffraction and using an electronic scanning microscope.

The results of ICP and AAS analyses of aqueous solutions showed that the hydrochloric acid solution, in equilibrium with scheelite, was enriched with calcium and contained relatively low concentrations of tungsten. It was found that the calcium concentration in quenched solutions does not depend on redox conditions ($f(O_2)$) (Fig. 1), but it increases with increasing HCl concentration in the initial solution, and the angle of inclination of $\lg mCa_{aq}/mHCl_{init}$ is close to 1.0 ± 0.1 at 400 and 500° C. The calcium content in the initial solutions of 0.01, 0.0316, 0.1 and $0.316m$HCl was insignificant and amounted to 3.0, 2.2, 1.9 and 16×10^{-5} mol/kg H_2O, respectively.

The concentration of tungsten in solutions after the experiments, on the contrary, did not depend much on mHCl$_{init}$, but increased with a temperature change from 400 to 500° C on average by one order of magnitude (10 times). The influence of redox conditions ($f(O_2)$) on the m W_{aq} was established, but it was ambiguous.

The scheelite, used in the experiments, was initially white in color, but it had changed during the experiment. If, in the runs containing $0.01m$HCl, the white color was preserved or a pale yellowish color appeared, then with an increase in HCl concentration, a color change was observed from light blue in 0.0316 m HCl to dark blue, almost black, in $0.316m$HCl (Table 1). The intensity of the dark coloration increased with a decrease in $f(O_2)$ from Cu_2O-CuO to CoCoO buffer.

Table 1. Color of solid phases after the run.

T, °C	Buffer	$\lg fO_2$ (Па)	Concentration HCl, mol/кg H_2O			
			0.01	0.0316	0.1	0.316
400	Co-CoO	-23.768	**W**+B	W+B	W+B	B+V
400	Ni-NiO	-22.423	**W**	**W**+B	**W**+B	W+B+V
400	Fe_3O_4-Fe_2O_3	-18.600	**W**+Y	**W**+Y+B	**W**+B	W+**B**+V
400	Cu_2O-CuO	-6.401	**W**	**W**+B	**W**+B	W+**B**
500	Ni-NiO	-17.706	**W**	W+Y+B	W+B+V	W+B+V
500	Co-CoO	-19.089	**W**+B	W+B	W+**B**	W+**B+V**
500	Cu_2O-CuO	-3.567	**W**+B	W+B	W+**B**	W+**B**

W – white, B – black, V – dark - blue, Y – yellow; bold letters – a lot of crystals; $CaWO_4$ – white ; WO_3 – lemon yellow; $WO_{2.9}$ – blue; $WO_{2.72}$ – red-violet; Ca_xWO_3, где x<0.1 – from purple to dark blue (Zelikman, Nikitina, 1978).
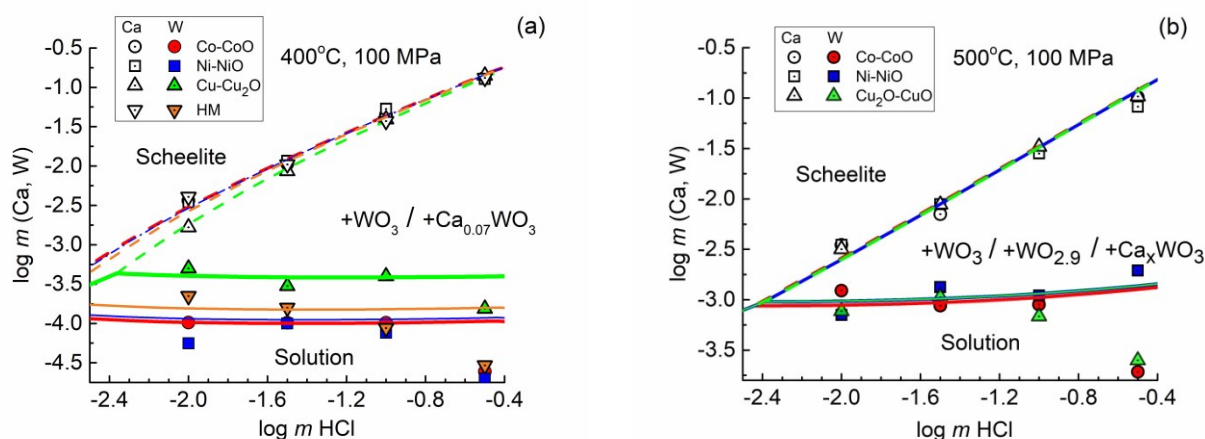

Fig.1. Influence of mHCl on the content of m W and Ca in a solution in equilibrium with scheelite at 400 (a) and 500° C (b), P = 100 MPa and oxygen fugitivity given by various metal-oxide buffers, according to experimental (symbols) and calculated (lines) data.

Examining the run solid products on a scanning electron microscope, it was found that in the entire studied range of HCl concentrations from 0.01 to 0.316m, scheelite dissolves incongruently. In relatively dilute solutions containing from 0.01 to 0.0316mHCl, insignificant amounts of tungsten oxides, WO_3 and (or) WO_{3-x}, are found in the run products, along with scheelite. In solutions containing 0.1 to 0.316 m HCl, the formation of calcium tungsten bronzes (CTB) Ca_xWO_3 is observed, the average composition of which corresponds to the formula $Ca_{0.07}WO_3$.

The yellow color of the run products indicates the presence of WO_3 crystals, dark blue indicates tungsten bronzes. The black color of crystals in experiments with Co/CoO and Ni/NiO buffers may be associated with the presence of non-stoichiometric tungsten oxides. According to the data (Wriedt, 1990) in the temperature range 400-500° C the stable oxide phases are WO_3, $WO_{2.9}$ (or $W_{20}O_{58}$) and WO_2.

Using the values of free energies for these tungsten oxides (Chase, 1998), we calculated the equilibrium values of $f(O_2)$. According to the calculations carried out, WO_3 is known to be stable only at Cu_2O/CuO buffer, whereas at f (O_2) the stable phase given by the Co/CoO buffer is $WO_{2.9}$ (or $W_{20}O_{58}$).

Based on the analysis of existing data on the thermodynamic properties of scheelite and tungsten oxides, calculations were performed in a system simulating the dissolution of scheelite in hydrochloric acid solutions at 400 and 500° C, 100 MPa and fO$_2$) in the range from Co-CoO to Cu_2O-CuO buffers (Fig. 1). Species of an aqueous solution were used in the calculations: H_2O, H^+, OH^-, Cl^-, HCl^0, Ca^{2+}, $CaCl^+$, $CaCl_2^0$, $CaOH^+$, WO_4^{2-}, HWO_4^-, $H_2WO_4^0$.

Calculations were carried out according to the Gibbs program (Shvarov, 2007). Individual coefficients of species activity were calculated using the extended Debye-Hückel equation (Akinfiev et al., 2020). The total concentrations of Ca and W in solutions were calculated in molar concentrations.

The dimensional parameter (effective ion radius) for all charged species is assumed to be 4.5 Å (Rafalsky, 1973). Calculations have shown that under Cu_2O-CuO buffer conditions ($f(O_2)$ = 3.98·10^{-7} Pa) at 400° C, the field of scheelite congruent solubility is at HCl concentrations below 4.34·$10^{-3}m$). At 500° C and Cu_2O-CuO buffer fugitivity ($f(O_2)$ = 2.71·10^{-4} Pa), the field of scheelite congruent solubility is at HCl concentrations below 4.08·$10^{-3}m$. The solubility of Sch in H_2O, according to calculations, is 2.78·10^{-6} and 2.93·10^{-6} mol kg^{-1} H_2O. An increase in HCl concentration leads to the deposition of WO_3 from the solution. Complete replacement of Sch with the newly formed WO_3 phase takes place in solutions

containing mHCl > 0.42 at 400° C and 0.56 at 500° C.

Under conditions controlled by Fe_3O_4-Fe_2O_3 buffer ($f(O_2)$ = 2.51·10^{-19} Pa) at 400° C , Ni-NiO buffer ($f(O_2)$ = 3.78·10^{-23} Pa) at 400°C and 1.97·10^{-18} Pa at 500°C and Co-CoO buffer ($f(O_2)$ = 1.71·10^{-24} Pa) at 400°C and 8.16·10^{-20} Pa at 500 °C, scheelite dissolves with the formed CTB. The field of scheelite congruent solubility, as well as with Cu_2O-CuO buffer, is rather narrow and limited by mHCl < 2·10^{-3}. In solutions containing mHCl > 0.36, at a given ratio of scheelite / solution = 0.18mol Sch / 1000g H_2O, at 400° C, the stable phase is WO_3. According to calculations, the effect of solutions containing mHCl > 0.56 on 0.22 mol Sch at 500° C and (fO$_2$) (Ni-NiO) leads to the formation of WO_3, whereas with Co-CoO buffer, $WO_{2.9}$ oxide is stable.

Thermodynamic modeling of Sch in 0.001 – 1.0mKCl solutions was carried out on the lines of hydrolysis equilibrium of microcline (Mic) with quartz (Qtz) and muscovite (Ms). It is shown that the dissolution of Sch in KCl solutions at 400 and 500° C occurs congruently and the oxygen fugitivity (Co/Co, Ni/NiO and Cu_2O/CuO buffers) does not affect the calculation results.

According to calculations, the main contribution to the solubility of scheelite is made by the particle HWO_3-.The increase in the solubility of scheelite is mainly associated with an increase in the ionic strength of the solution (Bryzgalin, 1976). The calculation results are comparable with the experimental data of R.P. Forster (1977) (Fig. 2).
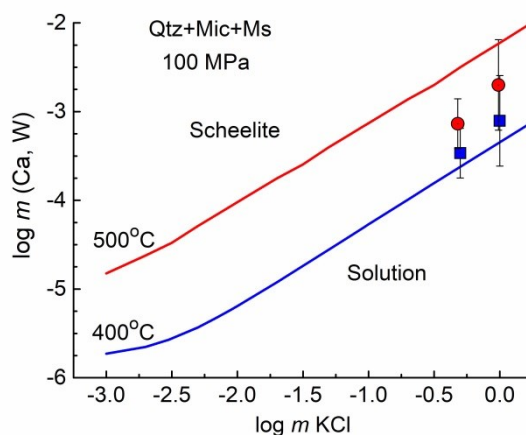

Fig.2. Influence of mKCl on the content of mW and mCa in a solution in equilibrium with scheelite under conditions controlled by quartz-microcline-muscovite buffer at 400 and 500° C, 100MPa and oxygen fugitivity given by nickel-bunsenite (NNO) buffer according to experimental (Foster, 1977) symbols: square-400° C, round-500° C and calculated (line) data.

As a result of the conducted studies, data on the of oxygen fugitivity $f(O_2)$ effect and acidity (mHCl) on the solubility of scheelite ($CaWO_4$) at 500 and 400° C and 100 MPa were obtained. The conducted studies have shown that the dissolution of scheelite in HCl solutions takes place incongruently with the

formation of tungsten oxides WO_3, $WO_{2.9}$ and calcium tungsten bronzes, the average composition of which corresponds to the formula $Ca_{0.07}WO_3$. An increase in HCl concentration contributes to the yield of WO_3 (or WO_{3-x}). An increase in temperature reduces the yield of WO_3, which is associated with an increase in the solubility of this phase.

Based on the analysis of the experimental data obtained, the free energies of the formation of tungsten oxides WO_3, $WO_{2.9}$, scheelite and calcium tungsten bronze are calculated.

Using mutually consistent thermodynamic data, the solubility of Sch in HCl and KCl solutions was calculated. It is shown that scheelite has a wide range of congruent solubility in salt systems.

References

1. Bryzgalin O.V. On the solubility of tungstic acid in aqueous salt solutions at high temperatures // Geochemistry. 1976. No.6. P. 864-870.
2. Zelikman A.M., Nikitina L.S. Wolfram. M.: Metallurgy. 1978. 272 p.
3. Rafalsky R.P. Hydrothermal equilibria and processes of mineral formation. M.: Nauka. 1973. 288 p. Free book site: http://www.geokniga.org/books/7820 (in Russian).
4. Shvarov Yu.V. On thermodynamic models for real solutions. *Geochem. Intern.*, 2007. 45, No 6, P. 606-614.
5. Akinfiev N.N., Korzhinskaya V.S., Kotova N.P., Redkin A.F., Zotov A.V. Niobium and tantalum in hydrothermal fluids: Thermodynamic description of hydroxide and hydroxofluoride complexes // Geochimica et Cosmochimica Acta. 2020. V.280. P. 102-115.
6. Chase Jr. M.W. NIST-JANAF Thermochemical Tables, 4th Edition, American Institute of Physics. 1998. Part 1. 1961 p.
7. Foster R.P. Solubility of scheelite in hydrothermal chloride solutions // Chemical Geology. 1977. V. 20(1). P. 7-43.
8. Khodokovskiy I.L., Mishin I.V. Solubility products of calcium molybdate and calcium tungstate; ratio of powellite to scheelite mineralization under hydrothermal conditions // International Geology Review. 1971. V. 13. №. 5. P. 760-768.
9. Wood S. A. and Samson I. M. The hydrothermal geochemistry of tungsten in granitoid environments: I. Relative solubilities of ferberite and scheelite as a function of T, P, pH, and m_{NaCl} // Economic Geology and the Bulletin of the Society of Economic Geologists. 2000. V. 95(1), P. 143-182.
10. Wriedt H.A. The O-W (Oxygen-Tungsten) system // Bulletin of Alloy Phase Diagrams. 1989. V. 10(4). P. 368-384.

Tauson V.L., Lipko S.V., Smagunov N.V., Babkin D.N., Belozerova O.Yu. Cocrystallization of main impurity elements and noble metal admixtures in sphalerite in hydrothermal systems: the effect of sulfur fugacity. UDC: 550.42+553.21/24+549.321.1

A.P. Vinogradov Institute of Geochemistry, SB RAS, Irkutsk
vltauson@igc.irk.ru

Abstract. The sulfur fugacity effect on the partition and cocrystallization coefficients of main metal impurities (Me) and several noble metals (NM=Au, Ag, Pt, Pd) in sphalerite has been studied at 450° C and 1 kbar pressure. $D_{Me/Zn}$ values increase with fS_2 lowering for Fe and Co and, to a minor degree, for Mn. Mercury behavior is caused by its change to neutral form Hg_{aq}° under reducing conditions. Being best compatible in sphalerite among other Me at more high sulfur fugacity, Hg is no longer incorporated into sphalerite at $fS_2 < \sim 10^{-7}$ bar. As regards Au, the data on its low solubility in sphalerite under given T, P parameters are confirmed as well as low $D_{Au/Zn}$ value (~ 0.002). Silver and Pd are distributed evenly and determined reliably by EPMA and LA-ICP-MS in numerous points of analysis (>70%). Palladium concentrations of 330-460 ppm are obtained at 0.05-2.55 wt.% Fe in sphalerite; $D_{Pd/Zn}$ is found to be unexpectedly high (80±30) for the conditions studied ($fS_2 \sim 10^{-2}$ bar). Palladium looks like a highly compatible element in sphalerite and may be qualified as a perspective indicator of NM presence in paleofluids. However, the retention of Pd concentration in solution prepared from fluid captured by the sampler appears relevant. Silver contents in sphalerite under the conditions studied are determined at a level of 100-300 ppm. The higher contents (340-730 ppm) observed in the systems with various Me impurities are possibly due to the formation of Me cluster defects including Ag.

Keywords: distribution; cocrystallization; sulfur fugacity; hydrothermal solution; sphalerite; trace elements; noble metals

Introduction. Despite widespread application of new analytical methods and technologies, the nature of elements behavior in endogenous and exogenous geochemical processes remains largely unclear. Reconstruction of paleofluids using minerals of variable composition was theoretically justified more than 40 years ago (Urusov, 1980; Chernyshev, 1980), however, there are still practically no systematic studies of the distribution and cocrystallization coefficients of main typomorphic impurity elements in ore minerals for hydrothermal domain of parameters. Despite the importance of potential results (van Hinsberg et al., 2010), such studies hardly attract practical researchers due to their labor inputs and complexity of organization: they require identification of factors affecting cocrystallization and speciation of the elements both in the mineral and in the fluid, which is in equilibrium with it. Earlier, in hydrothermal experiments with thermogradient growth of mixed sphalerite crystals and internal fluid sampling at 450° C and a pressure of 1 kbar, the values of distribution and

cocrystallization coefficients of Mn, Fe, Co, Ni, Ag, Cd and Hg were obtained (Tauson et al., 2019). Within the studied interval of ferrugenosity of sphalerite (1-3 wt.%) its effect on cocrystallization coefficient of $D_{Me/Zn}$ was not observed. In the fore quoted work, elements with the most stable behavior of $D_{Me/Zn}$ under variation of physicochemical conditions (Fe, Mn, Co и Cd), and, thus, applicable for restoration of paleofluids composition were identified. Therefore, it was important to establish to what extent this constancy is maintained at low sulfur fugacity when sphalerite crystallizes together with pyrrhotite. Similar data for noble metals (NM) are also of interest. It was previously shown that cocrystallization coefficient of gold $D_{Au/Me}$, where Me = Zn+Fe, increases from ∼ 0.002 to 0.006 depending on the ferruginosity of sphalerite within multiphase hydrothermal system at 450°C and 1 kbar (Lipko et al., 2020).

Methods of experiment and analysis. The experimental technique for obtaining sphalerite crystals in the presence of Fe, Co, Ni, Cd, Mn and Hg impurities practically did not differ from that described in the above-mentioned work (Tauson et al., 2019), except for the composition of the batch, in which the main components were zinc sulfide, elemental iron and sulfur. Hydrothermal thermogradient synthesis of crystals was used in passivated titanium inserts at 450 °C and a pressure of 100 MPa (1 kbar) with a 15-degree temperature drop along the outer wall of the autoclave, in solutions based on ammonium chloride – 5 and 10 wt.% NH₄Cl, 8% NH₄Cl+2% HCl. Internal fluid sampling into perforated titanium traps was used. The experiment was performed in isothermal conditions for 4 days to homogenize the system, then at temperature drop for 20 days. Autoclaves were quenched in cold running water at a rate of ∼5 K/s. Solutions from the traps, after necessary chemical operations, were analyzed by atomic absorption spectrometry (AAS) on Perkin-Elmer devices (USA). Mercury analysis was carried out on the RA-915+ spectrometer. The obtained crystalline phases were analyzed by electron microprobe analysis (EMPA) on the Superprobe JXA-8200 unit (JEOL Ltd, Japan), a number of control measurements at low element contents, near EMPA detection limit, were performed by the LA-ISP-MS method on the Agilent 7500ce unit (Agilent Tech., Santa Clara, CA, USA) with NWR UP-213 laser ablation platform. At the same P, T parameters, distribution and cocrystallization of NM in the ZnS – Ag₂S – Au – Pt – Pd – (±Fe, S) – 2m NH₄Cl system were studied. Solutions from the traps were analyzed by the AAS method using extraction into organic phase in the case of Pt and Pd (Tauson et al., 2018).

Results and discussion. The experiments in the two-phase region "sphalerite+pyrrhotite" yielded crystals of sphalerite from dark brown to black, mainly represented by cubotetrahedra and twins, sometimes flattened in shape, up to 2.5 mm in size. Pyrrhotite crystals coexisting with them are short–prismatic hexagonal, non-magnetic, up to 2 mm in size. In systems with NM, in several experiments, along with transparent, light yellow crystals of sphalerite up to 3 mm in size, dark, opaque crystals in volume were formed. X-ray diffraction (unit cell parameter) and analytical studies have shown their complete structural and chemical identity with light differences, so the differences in color are not yet clear. EMPA data were processed according to the 1σ criterion, with the number of points for each sample being ∼50-80. Sulfur fugacity was determined by the equations from the research (Scott, Barnes, 1971), in which the argument is FeS content in sphalerite, coexisting with pyrrhotite or pyrite (points at –log fS₂ = 3.5, Fig. 1).
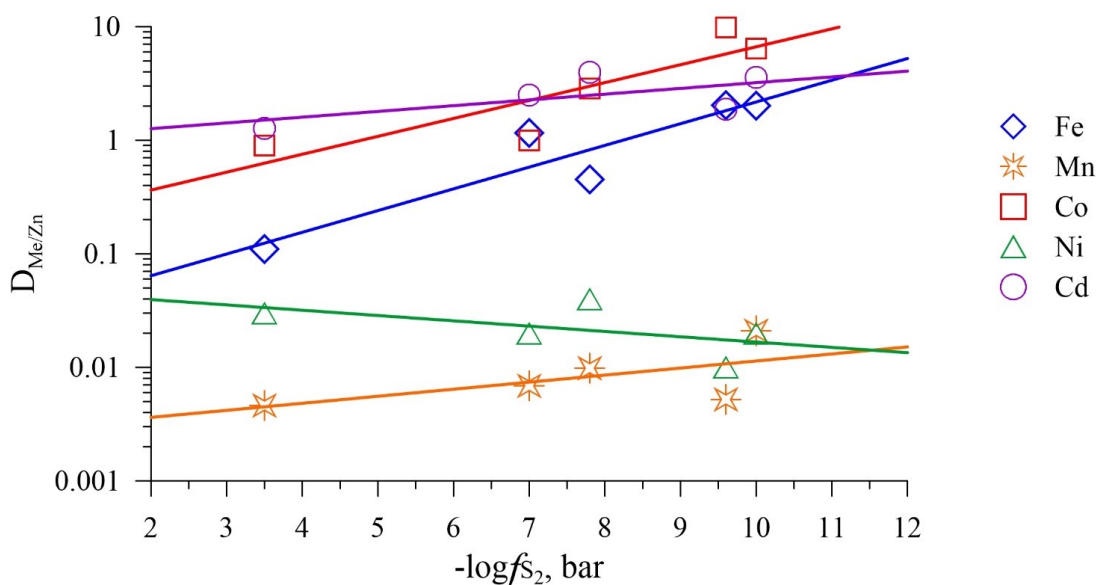

Fig. 1. Dependences of metallic impurities cocrystallization coefficients in sphalerite on sulfur fugacity in the system

Mercury was not found in sphalerite crystals at the lowest $f\mathrm{S}_2$, and its content in the fluid under these conditions also proved to be very low: 0.07–0.16 ppm. At the same time, $D_{\mathrm{Hg/Zn}}$ values obtained for it do not contradict the data we acquired earlier at higher $f\mathrm{S}_2$, which, however, are characterized by significant variance (Tauson et al., 2019). The behavior of mercury is explained by its transition to the neutral form of $\mathrm{Hg_{aq}}^0$ under reducing conditions, which is why it ceases to enter sphalerite at $f\mathrm{S}_2 < \sim 10^{-7}$, being the most well-compatible element in sphalerite under other conditions. With low sulfur activity, there is a slight increase in $D_{\mathrm{Mn/Zn}}$ - from 0.004 to 0.01; at the same time, Mn becomes a compatible element in sphalerite, and its content in it reaches 3 wt.%. Apparently, these are exactly the conditions under which high-manganese sphalerite and wurtzite could form in nature (Makeev, 1985). $f\mathrm{S}_2$ has practically no effect on Cd behavior ($D_{\mathrm{Cd/Zn}}$ equals on average 2.6 and 3.0 for low- and high-ferriferous sphalerites, respectively), so the appearance of Cd-enriched sphalerites in natural conditions is most likely due to the influence of medium acidity (Tauson et al., 2019). Ni is very poorly included in sphalerite under all conditions, and $D_{\mathrm{Ni/Zn}}$ somewhat decreases with a drop in sulfur fugacity (Fig. 1), although within reasonable error. Fe and Co are two elements that are equally affected (almost the same slope angles of the dependence to the $f\mathrm{S}_2$ axis) by sulfur fugacity – an increase in $D_{\mathrm{Me/Zn}}$ with its decrease (Fig. 1). Since there is a clear relationship between $D_{\mathrm{Me/Zn}}$ and the ratio of solubility products of the corresponding pure sulfides, then according to the general expression for cocrystallization coefficient (Smagunov et al., 2021), the most likely reason for the increase in $D_{\mathrm{Me/Zn}}$ Co and Fe is the rise in the complexation ratio of Zn and these elements in solution. Changes in $D_{\mathrm{Me/Zn}}$ with a decrease in $f\mathrm{S}_2$ for the elements previously identified as promising geochemical indicators (Fe, Mn, Co and Cd) are not dramatic, their noticeable increase is observed only for Fe and Co at the lowest $f\mathrm{S}_2$ ($<10^{-7.8}$ bar).

Investigation of NM distribution did not provide reliable data on Pt in sphalerite. Au was determined only using LA-ISP-MS at the level of 1.5±1 ppm, the corresponding $D_{\mathrm{Au/Zn}}$ was $\sim 2 \cdot 10^{-3}$, which does not contradict the data presented in the Introduction. Ag and especially Pd are distributed uniformly and are recorded by the EMPA in a large number of analysis points (>70%). Pd contents were 330-460 ppm with sphalerite ferruginosity from 0.05 to 2.55 wt.% Fe. Its cocrystallization coefficient turned out to be unexpectedly high (80±30) for the studied conditions of relatively high sulfur fugacity ($\sim 10^{-2}$ bar). According to these data, Pd is a highly coherent element in sphalerite. EMPA and LA-ICP-MS do not indicate the presence of any proper phases of Pd, but

the question of the preservation of its concentrations in solutions obtained from trapped fluids remains relevant. As for Ag, under the conditions of the test, its content in sphalerite is at the level of 100-300 ppm. In the transported sulfide material, individual thin plates are found, which, according to X-ray phase analysis, are acanthite/argentite ($\mathrm{Ag_2S}$) with admixtures of silver oxides. Therefore, these contents are most likely to be maximum under these conditions. Higher concentrations of Ag (340-2210 ppm) in sphalerite were observed in the multisystem, where all its main metallic impurities were present - Mn, Fe, Co, Ni, Ag, Cd and Hg (Tauson et al., 2019). At the same time, cocrystallization coefficient $D_{\mathrm{Ag/Zn}}$ averages 1.5, and the distribution coefficient (~ 30) indicates Ag coherence in sphalerite. However, the assumption that any elements (or element) raise Ag solubility in the solid phase cannot yet be confirmed, due to a limited data set. It is possible that higher Ag concentrations were observed in a system with a complete set of Me impurities due to the formation of cluster defects involving Ag by these metals.

In high-temperature tests (750-850 $^{\circ}$C) performed by methods of gas transport reaction and solution in a salt melt (Tonkacheev et al., 2015), in iron-free Mn and Cd-containing sphalerite (0.76 and 0.56 wt.%, respectively) determined 610±350 ppm Ag (EMPA), while Pt and Pd were practically absent (<MDL=30 ppb, LA-ISP-MS). Sphalerite with 1.73 wt.% Fe is heterogeneous in Ag, while Au, on the contrary, is evenly distributed, and its content is 234±34 ppm and reaches 3000±460 ppm in the presence of Mn, In, Se and Cd impurities. The chemical situation in these experiments is not clear and, obviously, does not correspond at all to the conditions of natural sphalerites formation.

Conclusion. We have previously experimentally demonstrated that in the course of reconstruction of paleofluids composition, the cocrystallization coefficient has an advantage over the distribution coefficient, as a simple ratio of element concentrations in a mineral and in a solution (Smagunov et al., 2021). With functioning "complex solvent" model (Chernyshev, 1980), the cocrystallization coefficient is less variable due to chemical similarity of cocrystallizing elements. The data obtained in the present study, in general, confirm this conclusion by the example of impurity elements in sphalerite with extensive variations in sulfur fugacity. Changes in $D_{\mathrm{Me/Zn}}$ with a decrease in $f\mathrm{S}_2$ for elements previously identified as promising geochemical indicators (Fe, Mn, Co and Cd) are not dramatic, their noticeable increase is observed only for Fe and Co at the lowest $f\mathrm{S}_2$ ($<10^{-7.8}$ bar). Data on noble metals distribution show that Pd in sphalerite can be a promising indicator of fluid composition, but this issue requires special study due to the

uncertainty of its position in the mineral structure (or outside it).

References

1. Makeev A.B. Isomorphism of manganese and cadmium in sphalerite. – L.: Nauka, 1985. – 127 p.
2. Tauson V.L., Smagunov N.V., Lipko S.V., Babkin D.N., Belozerova O.Yu. Cocrystallization of impurity elements in sphalerite according to hydrothermal experiments // Proceedings of the All-Russian Annual Seminar on Experimental mineralogy, petrology and geochemistry. Moscow (April 16-17, 2019) / ed. O.A. Lukanin. – M.: GEOKHI RAS, 2019. – P.180 – 183.
3. Urusov V.S. Energetic formulation of the problem of equilibrium cocrystallization from an aqueous solution // Geokhimiya. – 1980. – No. 5. – P. 627-644.
4. Chernyshev L.V. On the theory of hydrothermal equilibria of minerals of variable composition // Geokhimiya. – 1980. – No. 6. – P. 787-797.
5. Lipko S., Tauson V., Bychinskii V. Gold partitioning in a model multiphase mineral-hydrothermal fluid system: distribution coefficients, speciation and segregation // Minerals. – 2020. – V.10. – No.10. – Art. 890.
6. Scott S.D., Barnes H.L. Sphalerite geothermometry and geobarometry // Econ. Geol. – 1971. – V. 66. – No. 4. – P. 653-669.
7. Smagunov N., Tauson V., Lipko S., Babkin D., Pastushkova T., Belozerova O., Bryansky N. Partitioning and surficial segregation of trace elements in iron oxides in hydrothermal fluid systems // Minerals. – 2021. – V. 11. – No. 1. – Art. 57.
8. Tauson V.L., Lipko S.V., Smagunov N.V., Kravtsova R.G. Trace element partitioning dualism under mineral-fluid interaction: Origin and geochemical significance // Minerals. – 2018. – V. 8. – No. 7. – Art 282.
9. Tonkacheev D.E., Chareev D.A., Abramova V.D., Minervina E.A., Yudovskaya M.A., Tagirov B.R. Sphalerite as a matrix for noble, non-ferrous metals and semi-metals: a EPMA and LA-ICP-MS study of synthetic crystals // Proc. 13th SGA Biennial Meeting on Mineral Resources in a Sustainable World, august 24-27, 2015, Nancy, France. – 2015. – V.2. – P. 847 – 849.
10. Van Hinsberg V.J., Migdisov A.A., Williams-Jones A.E. Reading the mineral record of fluid composition from element partitioning // Geology. – 2010. – V. 38. – No. 9. – P. 847-850.

Korzhinskaya V.S., Kotova N.P. Effect of solution composition and temperature on solubility of tantalum and niobium oxides, tantalite and pyrochlore in fluoride-chloride fluids.

Institute of Experimental Mineralogy RAS, Chernogolovka, Moscow district vkor@iem.ac.ru, kotova@iem.ac.ru

Abstract. Concentration and temperature dependences of tantalum and niobium oxides, as well as natural minerals pyrochlore $(Ca, Na)_2 (Nb, Ta)_2 O_6 (O, OH, F)$ and tantalite $(Mn, Fe)(Ta, Nb)_2O_6$ solubility in mixed (m HF + m HCl) fluids have been experimentally studied. The initial concentration of HF varied from 0.01 to 2 m, and the concentration of HCl remained constant and was 0.5 m. The obtained data allowed us to estimate the equilibrium contents of niobium and tantalum in (HF + 0.5m HCl) solutions at $T = 300 – 550^o$ C, P = 100 MPa in the presence of an oxygen buffer Co-CoO. The effect of temperature on the solubility of Ta and Nb oxides and minerals of pyrochlore and tantalite has been established. A comparative analysis of the Nb and Ta equilibrium contents in (m HF + m HCl) fluids for niobium and tantalum oxides and natural minerals pyrochlore and tantalite was carried out.

Keywords: experiment, niobium and tantalum oxides, tantalite, pyrochlore, hydrothermal solubility, fluoride - chloride solutions

Experimental studies of the ore minerals solubility under controlled physico-chemical parameters, necessary for the creation of reliable databases used to determine the predominant forms of ore element transfer, assessment of their thermodynamic properties and subsequent construction of quantitative models of ore elements fractionation in the natural environment, determination of conditions for the formation of rare metal deposits associated with granites of various alkalinity, including, and with Li-F granites, they become of paramount importance.

Currently, the world-wide data on the solubility of Ta and Nb minerals under T-P-X-$f(O_2)$ conditions corresponding to magmatic and hydrothermal processes of mineral - and ore formation are clearly insufficient to determine the role of hydrothermal-metasomatic processes in the genesis of rare metal deposits. Therefore, the estimation of the limiting concentrations of ore elements in hydrothermal solutions in a wide range of T-P-X parameters necessary for constructing a quantitative model of the ore formation process remains an actual problem of ore genesis.

This work is a continuation of systematic experimental studies on the dissolution, transfer and deposition of Ta and Nb minerals by hydrothermal fluids (HF + HCl) (Korzhinskaya, Kotova, 2016, 2017, 2020), which presents data on the behavior of niobium (β-Nb_2O_5) and tantalum (β-$Ta_2 O_5$) oxides, as well as natural minerals pyrochlore $(Ca, Na)_2(Nb, Ta)_2O_6(O, OH, F)$ and tantalite $(Mn, Fe)_2 (Ta, Nb)_2O_6$

when they are dissolved in (mHF+0.5mHCl) solutions at 300 – 550° C and 100 MPa (Co-CoO buffer). The initial concentration of HF varied from 0.01 m to 2 m, and the concentration of HCl remained constant and was 0.5 m. The experiments were carried out on a high-pressure hydrothermal apparatus in platinum ampoules sealed by electric arc welding. The analysis of quenching solutions was carried out by the most precise and modern methods of inductively coupled plasma ICP/MS, ICP/AES and AAS. The phase composition of the solid products was studied by powder X-ray diffraction and using an electronic scanning microscope.

In Fig. 1a, b are the results of experiments on the study of the concentration dependences of niobium and tantalum equilibrium contents during the dissolution of niobium oxide and pyrochlore (Fig.1a), tantalum oxide and tantalite (Fig. 1b) in (mHF + 0.5 mHCl) solutions at 300° C and 100 MPa and Co-CoO buffer conditions. Analysis of the data obtained showed that when Nb_2O_5 and pyrochlore are dissolved in a solution with a low concentration of HF: (0.01 mHF+0.5 mHCl), the equilibrium niobium content is the same and is (n 10^{-5} m). With an increase in the concentration of F-ion in (0.1 mHF+0.5 mHCl) and (0.5 mHF+0.5 mHCl) solutions the solubility of Nb_2O_5 increases and becomes greater than for pyrochlore by almost 2 orders of magnitude, and pyrochlore solubility it practically does not change. In (2 m + 0.5m HCl) solution, the equilibrium niobium content for both niobium oxide and pyrochlore reaches significant values (n·10^{-1} m) quite sufficient for real mass transfer of niobium by hydrothermal solutions.

During experiments on the solubility of tantalum oxide and tantalite in mixed solutions (mHF + 0.5 mHCl) (Fig. 1b), it was found that at 300° C and low concentrations of fluorides (0.01 mHF + 0.5 mHCl), the equilibrium tantalum content for Ta_2O_5 is less than the detection limit ($\leq$ n 10^{-7} mol/kg H_2O), and for tantalite is n $10^{-6.5}$ m. But with an increase in the HF concentration, the Ta content increases sharply when Ta_2O_5 is dissolved and in (2 mHF + 0.5 mHCl) solution reaches values of 10^{-2} m. It was found that at 300° C, as well as at 550° C and 100 MPa in fluoride-chloride (mHF + 0.5 mHCl) solutions, tantalum oxide has a clearly expressed positive dependence of solubility on the concentration of F-ion, in logarithmic units close to linear (Kotova, 2017). When tantalite is dissolved in high concentrations fluoride-bearing aqueous solutions: (0.5 mHF+0.5 mHCl) and (1 mHF+0.5 mHCl), the Ta content in the solution at 300° C increases to n*10^{-2} mol/kg H_2O that is, it has the same solubility as tantalum oxide.

The temperature dependences of the equilibrium contents of niobium and tantalum during the dissolution of Nb_2O_5, Ta_2O_5, pyrochlore and tantalite in (mHF + 0.5 mHCl) solutions are shown in Fig. 2a, b and 3a, b. The experimental studies did not show clearly expressed unambiguous dependences of the temperature effect on the solubility of Nb and Ta compounds in (m HF + 0.5 m HCl) solutions of different concentrations. It was found that when Nb_2O_5 is dissolved in (0.1 mHF + 0.5 mHCl) solutions with a low concentration of HF at 300° C and 100 MPa, the equilibrium niobium content is 1.5 orders of magnitude higher than that of pyrochlore, 3.5 orders of magnitude higher than that of tantalite, and is n·10^{-4} m (Fig. 2a). The temperature change does not significantly affect solubility of niobium oxide in (0.1mHF + 0.5m HCl) solutions. At the same time, positive temperature dependence of solubility is observed for pyrochlore and tantalite. At 550° C and 100 MPa, the niobium content for pyrochlore increases by 1 order of magnitude and amount to n·10^{-3} m. For tantalite, the equilibrium niobium content is n·10^{-5} m. In solutions with a high F-ion content (1 mHF+0.5 mHCl) (Fig. 2b), the niobium oxide solubility increases by 1.5 orders of magnitude and amounts to n·10^{-2}m, which practically coincides with the niobium content when pyrochlore is dissolved at the same parameters (Korzhinskaya, Kotova, 2017).
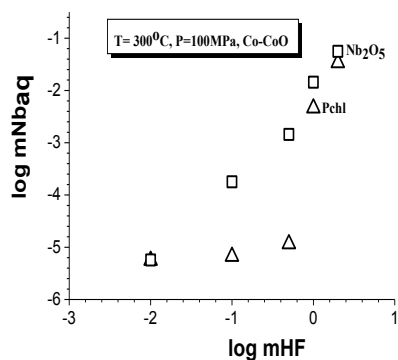

Fig. 1a. Concentration dependences of Nb_2O_5 and pyrochlore (Pchl) solubility in (mHF + 0.5m HCl) at 300°C, 100 MPa and Co-CoO buffer condition
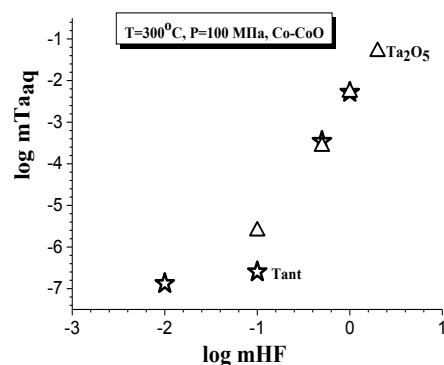
Fig. 1b. Concentration dependences of Ta_2O_5 and tantalite (Tant) solubility at 300°C, 100 MPa and Co-CoO buffer condition

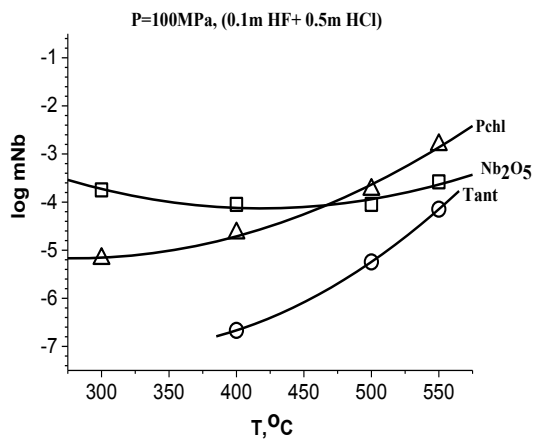**Institute of Experimental Mineralogy**

Fig. 2a. Temperature dependence of Nb_2O_5, pyrochlore and tantalite solubility in (0.1mHF+0.5mHCl) solution at 100 MPa and Co-CoO buffer condition
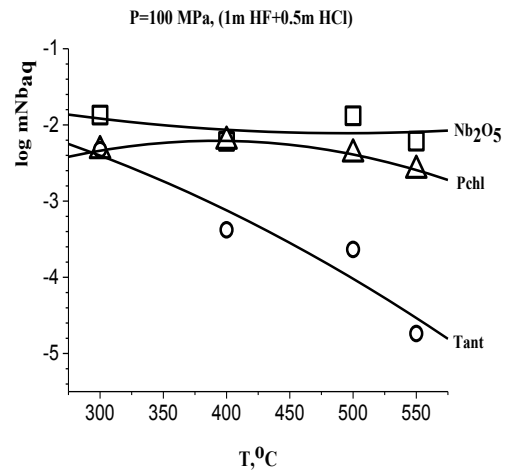
Fig. 2b. Temperature dependence of Nb_2O_5, pyrochlore and tantalite in (1mHF+0.5mHCl) solution at100 MPa and Co-CoO buffer condition
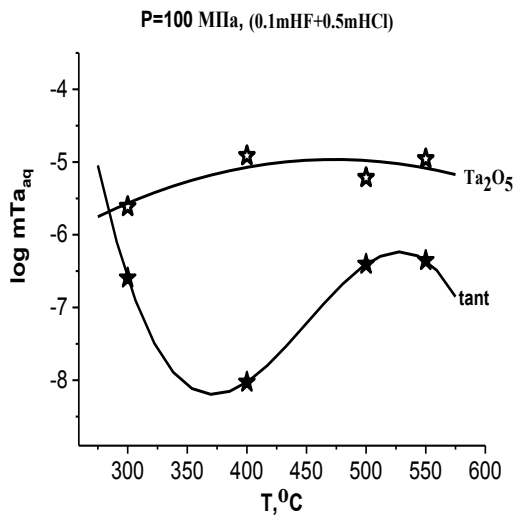

Fig. 3a. Temperature dependence of Ta2O5 and tantalite solubility in (0.1mHCl+0.5mHCl) at 100 MPa and Co-CoO buffer condition
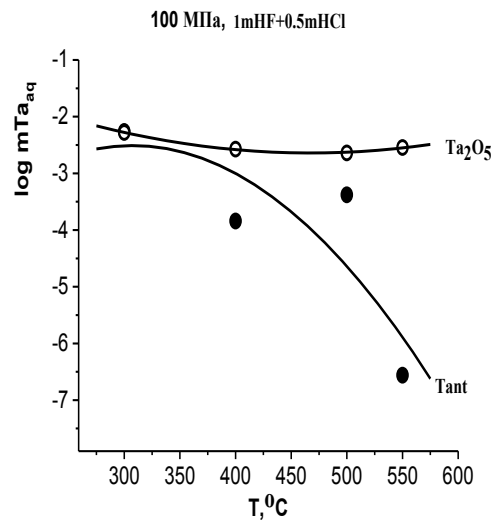
Fig. 3b. Temperature dependence of Ta2O5 and tantalite solubility in (1mHCl+0.5mHCl) at 100 MPa and Co-CoO buffer condition

The increase in temperature has no noticeable effect on the change in the solubility of pyrochlore and niobium oxide. For tantalite, an inverse temperature dependence of solubility is observed. At 300^oC and 100 MPa, the equilibrium niobium content is $n \cdot 10^{-3} \cdot m$, and at 550° C $– n \cdot 10^{-5}$ m.

In Fig. 3a, b, the temperature dependences of the equilibrium contents of tantalum during the dissolution of Ta_2O_5 and tantalite in (0.1mHF+0.5mHCl) and (1mHF+0.5mHCl) solutions are presented. When Ta_2O_5 is dissolved in (0.1mHF + 0.5m HCl) solution, the tantalum content is $n \cdot 10^{-5}$ m. Moreover, the temperature has little effect on the solubility of tantalum oxide. When tantalite is dissolved in (0.1 mHF + 0.5 mHCl) solution at 300, 500 and 550^oC and 100 MPa, the tantalum content is almost the same and amounts to

$n \cdot 10^{-6.5}$ m, which is 1.5 orders of magnitude less than for Ta_2O_5. At 400^oC, the equilibrium tantalum content is minimal (n•10-8 m), which is associated with the formation of the solid phase of the composition Mn_2TaO_3. At high concentrations of F-ion in (1 mHF + 0.5 mHCl) solutions, the equilibrium Ta content increases sharply when Ta_2O_5 is dissolved, and at 550° C and 100 MPa reaches values of $n \cdot 10^{-2.5}$ m, which is 4 orders of magnitude higher than tantalite. The temperature dependence of tantalum oxide solubility in (1 mHF + 0.5m HCl) solutions is practically absent. At the same time, when tantalite is dissolved in concentrated (1 mHF + 0.5 mHCl) fluoride-chloride solutions, an increase in temperature leads to a sharp decrease in the equilibrium tantalum content from $n \cdot 10^{-2}$ m at 300° C to $n \cdot 10^{-6.5}$ m at 550° C and 100 MPa.

Experimental results obtained by studying the solubility of pyrochlore, tantalite, Ta and Nb oxides in mixed fluids (mHF + 0.5 mHCl) allow us to conclude, that the hydrothermal transport of metals Ta and Nb in the quantities necessary for the formation of their industrial concentrations is favored only high concentrated fluoride-bearing aqueous solutions with an insignificant role of chloride solutions.

References

1. Korzhinskaya V.S., Kotova N.P. Experimental study of fluid composion (HF+HCl) influence on niobium behavior when dissolving pyrochlore and niobium oxide at T = 550 ° C, P = 1000 bar (Co-CoO buffer) // Experiment in Geosciences. 2016. Vol. 22. No .1 P. 61-63
2. Korzhinskaya V.S., Kotova N.P. Behavior of niobium and tantalum oxides, pyrochlore and tantalite in mixed aqueous solutions (HF + HCl) at T = 550°C and P = 1000 bar // Experiment in Geosciences. 2017. Vol. 23. No 1. P. 110-111
3. Korzhinskaya V.S., Kotova N.P. Temperature effect on the behavior of Ta and Nb during the dissolution of pyrochlore, tantalite, β - Ta_2O_5 and β - Nb_2O_5 in (HF+HCl) solutions // Experiment in Geosciences. 2020. Vol. 26. No 1. P. 93 – 95
4. Kotova N.P. Experimental study of the influence of fluid compound (HF + HCl) on tantalum oxide solubility at T = 550°C, P = 100 MPa // Experiment in Geosciences. 2017. V. 23. No 1. P. 108-109